

Testing Lepton Flavor Universality and CKM Unitarity with Rare Pion Decays in the PIONEER experiment

W. Altmannshofer,¹ H. Binney,² E. Blucher,³ D. Bryman,^{4,5} L. Caminada,⁶
 S. Chen,⁷ V. Cirigliano,⁸ S. Corrodi,⁹ A. Crivellin,^{6,10,11} S. Cuen-Rochin,¹²
 A. Di Canto,¹³ L. Doria,¹⁴ A. Gaponenko,¹⁵ A. Garcia,² L. Gibbons,¹⁶ C. Glaser,¹⁷
 M. Escobar Godoy,¹ D. Göldi,¹⁸ S. Gori,¹ T. Gorringer,¹⁹ D. Hertzog,² Z. Hodge,²
 M. Hoferichter,²⁰ S. Ito,²¹ T. Iwamoto,²² P. Kammel,² B. Kiburg,¹⁵ K. Labe,¹⁶
 J. LaBounty,² U. Langenegger,⁶ C. Malbrunot,⁵ S.M. Mazza,¹ S. Mihara,²¹ R. Mischke,⁵
 T. Mori,²² J. Mott,¹⁵ T. Numao,⁵ W. Ootani,²² J. Ott,¹ K. Pachal,⁵ C. Polly,¹⁵
 D. Počanić,¹⁷ X. Qian,¹³ D. Ries,²³ R. Roehnel,² B. Schumm,¹ P. Schwendimann,²
 A. Seiden,¹ A. Sher,⁵ R. Shrock,²⁴ A. Soter,¹⁸ T. Sullivan,²⁵ M. Tarka,¹ V. Tischenko,¹³
 A. Tricoli,¹³ B. Velghe,⁵ V. Wong,⁵ E. Worcester,¹³ M. Worcester,²⁶ and C. Zhang¹³

¹*Santa Cruz Institute for Particle Physics (SCIPP),*

University of California Santa Cruz, 1156 High street, Santa Cruz (CA) 95064 USA

²*Department of Physics, University of Washington,*

Box 351560, Seattle, Washington 98195 USA

³*Enrico Fermi Institute and Department of Physics,*

University of Chicago, 5720 South Ellis Avenue, Chicago, IL 60637 USA

⁴*Department of Physics & Astronomy,*

University of British Columbia 6224 Agricultural Road, Vancouver V6T 1Z1 Canada

⁵*TRIUMF, 4004 Wesbrook Mall, Vancouver V6T 2A3 Canada*

⁶*Paul Scherrer Institute, 5232 Villigen PSI Switzerland*

⁷*Department of Engineering Physics, Tsinghua University,*

30 Shuangqing Road, Haidian District, Beijing, 100084 P. R. China

⁸*Institute for Nuclear Theory, University of Washington, Seattle WA 98195-1550 USA*

⁹*Argonne National Laboratory, High Energy Physics Division,*

9700 S Cass Ave, Lemont, IL 60439 USA

¹⁰*Physik-Institut University of Zurich Winterthurerstrasse 190 CH-8057 Zurich Switzerland*

¹¹*Division of Theoretical Physics, CERN,*

Espl. des Particules 1, 1211 Meyrin Switzerland

¹²*Tecnológico de Monterrey, School of Engineering and Sciences,*

Blvd. Pedro Infante 3773 Pte, Culiacan 80100 Mexico

¹³*Physics Department, Brookhaven National Laboratory, Upton, NY, 11973 USA*

¹⁴*PRISMA+ Cluster of Excellence and Johannes Gutenberg Universität Mainz,*

Institut für Kernphysik, J.-J.-Becher-Weg 45, 55128 Mainz Germany

¹⁵*Fermi National Accelerator Laboratory (FNAL),*

P.O. Box 500, Batavia IL 60510-5011 USA

¹⁶*Department of Physics, Cornell University,
109 Clark Hall, Ithaca, New York 14853 USA*

¹⁷*Department of Physics, University of Virginia, P.O. Box 400714,
382 McCormick Road, Charlottesville, VA 22904-4714 USA*

¹⁸*ETH Zurich, Main building, Rämistrasse 101, 8092 Zurich Switzerland*

¹⁹*Department of Physics and Astronomy, University of Kentucky,
505 Rose Street Lexington, Kentucky 40506-0055 USA*

²⁰*Albert Einstein Center for Fundamental Physics,
Institute for Theoretical Physics, University of Bern,
Sidlerstrasse 5, 3012 Bern Switzerland*

²¹*KEK, High Energy Accelerator Research Organization,
1-1, Oho, Tsukuba-city, Ibaraki 305-0801 Japan*

²²*International Center for Elementary Particle Physics (ICEPP),
The University of Tokyo, 7-3-1 Hongo, Bunkyo-ku, Tokyo 113-0033 Japan*

²³*Department of Chemistry – TRIGA site,
Johannes Gutenberg University Mainz,
Fritz-Strassmann-Weg 2, 55128 Mainz Germany*

²⁴*C. N. Yang Institute for Theoretical Physics and Department of Physics and Astronomy,
Stony Brook University, Stony Brook, NY 11794 USA*

²⁵*Department of Physics and Astronomy, Elliott Building,
University of Victoria, Victoria, BC V8P 5C2 Canada*

²⁶*Instrumentation Division, Brookhaven National Laboratory, Upton, NY, 11973 USA*

ABSTRACT: The physics motivation and the conceptual design of the PIONEER experiment, a next-generation rare pion decay experiment testing lepton flavor universality and CKM unitarity, are described. Phase I of the PIONEER experiment, which was proposed and approved at Paul Scherrer Institut, aims at measuring the charged-pion branching ratio to electrons vs. muons, $R_{e/\mu}$, 15 times more precisely than the current experimental result, reaching the precision of the Standard Model (SM) prediction at 1 part in 10^4 . Considering several inconsistencies between the SM predictions and data pointing towards the potential violation of lepton flavor universality, the PIONEER experiment will probe non-SM explanations of these anomalies through sensitivity to quantum effects of new particles up to the PeV mass scale. The later phases of the PIONEER experiment aim at improving the experimental precision of the branching ratio of pion beta decay (BRPB), $\pi^+ \rightarrow \pi^0 e^+ \nu(\gamma)$, currently at $1.036(6) \times 10^{-8}$, by a factor of three (Phase II) and an order of magnitude (Phase III). Such precise measurements of BRPB will allow for tests of CKM unitarity in light of the Cabibbo Angle Anomaly and the theoretically cleanest extraction of $|V_{ud}|$ at the 0.02% level, comparable to the deduction from superallowed beta decays.

Submitted to the Proceedings of the US Community Study
on the Future of Particle Physics (Snowmass 2021)

CONTENTS

I. Executive Summary	4
II. Introduction	5
III. Motivation	5
IV. PIONEER Experiment	8
A. Experiment Overview and Strategy	8
B. Conceptual Design	10
1. Beam	11
2. Active Target	12
3. Cylindrical Tracker	15
4. Liquid Xenon Calorimeter	15
5. Considerations on the Alternative LYSO Calorimeter	18
6. Trigger and Data Acquisition System	19
C. Simulations	22
1. ATAR Simulation	22
2. CALO Simulation	23
V. Sensitivity	25
A. $\pi \rightarrow e\nu$	25
B. Exotics	26
1. Massive neutrino searches $\pi^+ \rightarrow \ell^+ \nu_H$	26
2. Two body muon decay $\mu^+ \rightarrow e^+ X_H$	27
3. Other decays	28
C. Pion Beta Decay	29
VI. Planning for Realization of PIONEER	29
VII. Summary	31
Acknowledgments	31
References	31

I. EXECUTIVE SUMMARY

In recent years, there have been an increasing number of intriguing hints for lepton flavor universality violation (LFUV). Motivated by these indications of physics beyond the Standard Model, Phase I of the PIONEER experiment, approved at the Paul Scherrer Institute (PSI), aims to measure the charged-pion branching ratio to electrons vs. muons $R_{e/\mu}$ to 1 part in 10^4 , improving the current experimental result $R_{e/\mu}(\text{exp}) = 1.2327(23) \times 10^{-4}$ [1–5] by a factor of 15. This precision on $R_{e/\mu}$ will match the theoretical accuracy of the SM prediction allowing for a test of LFU at an unprecedented level, probing non-SM explanations of existing LFUV anomalies through sensitivity to quantum effects of new particles up to the PeV mass scale.

Phase II and III of PIONEER experiment aim to improve the experimental precision of the branching ratio of pion beta decay, $\pi^+ \rightarrow \pi^0 e^+ \nu(\gamma)$, currently at $1.036(6) \times 10^{-8}$, by a factor of three and an order of magnitude, respectively. The improved measurements of pion beta decay would allow one to extract $|V_{ud}|$ in a theoretically pristine manner. The ultimate precision of $|V_{ud}|$ is expected to reach the 0.02% level, which is comparable to the currently most precise deduction from superallowed beta decays, allowing for a stringent test of CKM unitarity. Furthermore, the PIONEER experiment will also improve the experimental limits [6–8] by an order of magnitude or more to a host of exotic decays probing for effects of heavy neutrinos and dark sector physics.

The conceptual design of the Phase-I PIONEER experiment includes a 3π -sr 25 radiation length liquid xenon calorimeter, a segmented low gain avalanche detector (LGAD) stopping target, a positron tracker, and other detectors. Compared to the previous generation of rare pion decay experiments, the 4-D (position and time) tracking capability of the LGAD-based active target allows for excellent separation of $\pi \rightarrow e\nu$ signal from vast amount of $\pi \rightarrow \mu \rightarrow e$ background ($\pi \rightarrow \mu\nu$ followed by $\mu \rightarrow e\nu\bar{\nu}$).

The PIONEER collaboration consists of participants from both the nuclear and particle physics communities including PIENU, PEN/PiBeta, and MEG/MEGII collaborations, as well as experts in rare kaon decays, low-energy stopped muon experiments, the muon $g - 2$ experimental campaign, high energy collider physics, neutrino physics, and other areas. The collaboration plans R&D in several critical areas including i) beam studies, ii) LGAD-based active target (sensor and readout electronics), iii) LXe calorimeter (optical sensor and optical segmentation), iv) DAQ, and v) trigger, in preparation for a technical design report. The collaboration is still developing and welcomes new members.

This Snowmass white paper describes the physics motivation and the conceptual design of the PIONEER experiment, and is prepared based on the PIONEER proposal [9] submitted to and approved with high priority by the PSI (CHRISP - Swiss Research InfraStructure for Particle physics) program advisory committee. Using intense pion beams, and state-of-the-art instrumentation and computational resources, the PIONEER experiment is aiming to take data at PSI by the end of this decade.

II. INTRODUCTION

Precise low-energy measurements of observables that can be very accurately calculated in the Standard Model (SM) offer highly sensitive tests of new physics (NP). In light of the existing intriguing hints for lepton flavor universality (LFU) violating NP [10–12], the ratio $R_{e/\mu} = \Gamma(\pi^+ \rightarrow e^+\nu(\gamma))/\Gamma(\pi^+ \rightarrow \mu^+\nu(\gamma))$ for pion decays to positrons relative to muons is especially promising: it is one of the most precisely known observables involving quarks within the SM and NP can even have (chirally) enhanced effects, making it an extremely sensitive probe of NP. However, while the uncertainty of the SM calculation for $R_{e/\mu}$ is very small (with relative precision 1.2×10^{-4} [13]), the current experimental world average is about a factor 15 less precise, limiting the NP reach.

A new experiment, PIONEER, is proposed at the Paul Scherrer Institute (PSI), where the highest intensity low energy pion beams are delivered. The Phase I of PIONEER [9], which has been approved by PSI (CHRISP - Swiss Research InfraStructure for Particle physics) program advisory committee with high priority, will bridge the gap of a factor 15 between theoretical and experimental precision for $R_{e/\mu}$. With measurements at the 0.01% level in precision, NP up to the PeV scale [14] may be revealed. Such precision would contribute to stringent tests of LFU in a context where several intriguing hints of LFU violation (LFUV) have emerged. In addition, it will allow extended searches for exotics such as heavy neutral leptons and dark sector processes. In later phases (II, III), PIONEER will also study pion beta decay $\pi^+ \rightarrow \pi^0 e^+\nu(\gamma)$ ultimately aiming at an order of magnitude improvement in precision to determine $|V_{ud}|$ in a theoretically pristine manner and test CKM unitarity, for which there is presently a $\approx 3\sigma$ tension [1]. PIONEER is an ambitious program that will span more than a decade of research activity at PSI. While we focus on the measurement of the $\pi \rightarrow e\nu$ branching ratio $R_{e/\mu}$ in this paper, the following sections discuss the theoretical motivation for pursuing the full rare pion decay program. Discussions of the PIONEER detector concepts, simulations, estimated sensitivities, and planning for realization follow.

III. MOTIVATION

While no particles or interactions beyond those of the SM have been observed so far, intriguing hints for LFUV have been accumulated in recent years [10–12]. In particular, the measurements of the ratios of branching ratios (Br) $R(D^{(*)}) = Br[B \rightarrow D^{(*)}\tau\nu_\tau]/Br[B \rightarrow D^{(*)}\ell\nu_\ell]$ [15–17], where $\ell = \mu, e$, and $R(K^{(*)}) = Br[B \rightarrow K^{(*)}\mu^+\mu^-]/Br[B \rightarrow K^{(*)}e^+e^-]$ [18–20] deviate from the SM expectation by more than 3σ [21–25] and 4σ [26–29], respectively. In addition, anomalous magnetic moments $(g-2)_\ell$ ($\ell = e, \mu, \tau$) of charged leptons are intrinsically related to LFUV, as they are chirality flipping quantities. Here, the longstanding discrepancy in $(g-2)_\mu$, just reaffirmed at the level of 4.2σ [30–32], can be considered as another hint of LFUV, since, if compared to $(g-2)_e$, the NP contribution scales with a

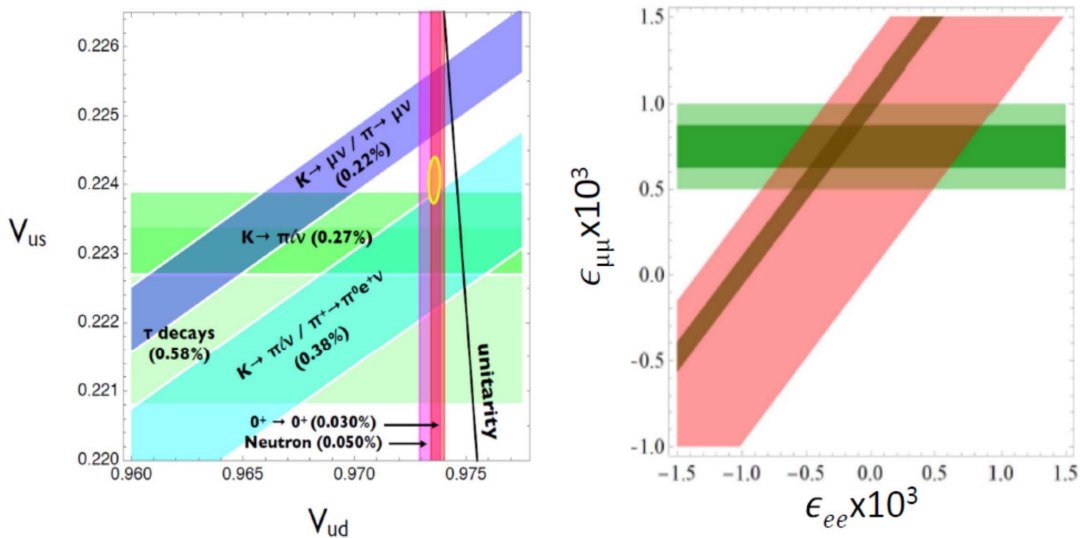


FIG. 1 – Left: Tensions in the first-row CKM unitarity test (see text) [12]. Right: Constraints (1σ) on modified $W\ell\nu$ couplings from CKM unitarity (green) and LFUV (red) (adapted from Ref. [39]). The light bands show the current status and the dark bands include the expected PIONEER sensitivity. The SM values of A_ℓ are assumed to be modified by $1 + \epsilon_{\ell\ell}$ where $\ell = e, \mu$.

power of the lepton mass [33, 34]. In addition, there is a hint for LFUV in the difference of the forward-backward asymmetries (ΔA_{FB}) in $B \rightarrow D^* \mu \nu$ vs $B \rightarrow D^* e \nu$ [35, 36]. As another possible indication of LFUV, CMS observed an excess in non-resonant di-electron pairs with respect to di-muons [37]. Furthermore, the possible deficit in first-row unitarity of the Cabibbo-Kobayashi-Maskawa (CKM) matrix, known as the Cabibbo angle anomaly (CAA) (see Fig. 1 (left)), can also be viewed as a sign of LFUV [38, 39]. For these reasons, there is very strong motivation for an upgraded $R_{e/\mu}$ experiment whose precision matches that of the SM prediction.

The branching ratio $R_{e/\mu} = \frac{\Gamma(\pi^+ \rightarrow e^+ \nu(\gamma))}{\Gamma(\pi^+ \rightarrow \mu^+ \nu(\gamma))}$ for pion decays to electrons over muons provides the best test of electron–muon universality in charged-current weak interactions. In the SM, $R_{e/\mu}$ has been calculated with extraordinary precision at the 10^{-4} level as [13, 40, 41]

$$R_{e/\mu}(\text{SM}) = 1.23524(15) \times 10^{-4}, \quad (1)$$

perhaps the most precisely calculated weak interaction observable involving quarks.¹ In comparison, the current experimental precision [1–5]

$$R_{e/\mu}(\text{exp}) = 1.2327(23) \times 10^{-4}. \quad (2)$$

¹ Reference [14] estimates the uncertainty due to the unknown non-leading-logarithmic contributions of $O(\alpha^2 \log(m_\mu/m_e))$ in a different way compared to Ref. [13]. This leads to a larger total uncertainty, i.e., $R_{e/\mu}(\text{SM}) = 1.23524(19) \times 10^{-4}$.

is more than a factor of 15 worse. Because the uncertainty of the SM calculation for $R_{e/\mu}$ is very small and the decay $\pi^+ \rightarrow e^+\nu$ is helicity-suppressed by the $V - A$ structure of charged currents, a measurement of $R_{e/\mu}$ is extremely sensitive to the presence of pseudoscalar (and scalar) couplings absent from the SM. Comparison between $R_{e/\mu}$ in theory and experiment provides a stringent test of the e - μ universality of the weak interaction; a disagreement with the theoretical expectation would unambiguously imply the existence of NP. With the PIONEER Phase I physics goal of improving $R_{e/\mu}$ experimental precision by a factor of 15 to 0.01% level, NP at the PeV scale can be probed [14], even up to several PeV in specific models such as leptoquarks. Assuming that LFUV originates from modified $W\ell\nu$ couplings, the determination of CKM elements will also be affected. Importantly, beta decays have an enhanced sensitivity to a modified $W\mu\nu$ coupling, due to a CKM enhancement by $|V_{ud}/V_{us}|^2 \sim 20$. Such a modification of the $W\ell\nu$ couplings would also affect $R_{e/\mu}$, albeit for a different flavor combination (see Fig. 1 (right)). This connection provides further motivation for an improved $R_{e/\mu}$ measurement, especially because the sensitivity to LFUV would be comparable to future improved constraints from beta decays.

The significance of the CAA, a 3σ tension with the CKM unitarity illustrated in Fig. 1 (left) [12, 42], depends crucially on experimental input quantities used for the extraction of CKM matrix elements as well as a number of theory corrections. The detector optimized for a next-generation $R_{e/\mu}$ experiment will also be ideally suited for a high-precision measurement of pion beta decay, which allows one to extract $|V_{ud}|$ in a theoretically pristine manner. The branching ratio for pion beta decay was most accurately measured by the PiBeta experiment at PSI [43–47] to be

$$\frac{\Gamma(\pi^+ \rightarrow \pi^0 e^+ \nu)}{\Gamma(\text{Total})} = 1.036 \pm 0.004 \text{ (stat)} \pm 0.004 \text{ (syst)} \pm 0.003 (\pi \rightarrow e\nu) \times 10^{-8}, \quad (3)$$

where the first uncertainty is statistical, the second systematic, and the third is the $\pi \rightarrow e\nu$ branching ratio uncertainty. While the pion beta decay provides the theoretically cleanest determination of the magnitude of the CKM matrix element $|V_{ud}|$, the current extraction of $|V_{ud}| = 0.9739(28)_{\text{exp}}(1)_{\text{th}}$ at 0.3% is not presently relevant for the CKM unitarity tests because superallowed nuclear beta decays provide a nominal precision of 0.03%. In order to make $\pi^+ \rightarrow \pi^0 e^+ \nu(\gamma)$ important for CKM unitarity tests, a two-step improvement in experimental precision is identified. As advocated in Ref. [48], the first step is a three-fold improvement in BRPB precision compared to Ref. [49] as proposed in PIONEER Phase II would allow for a 0.2% determination of $|V_{us}/V_{ud}|$ via improving the measurement of the ratio

$$R_V = \frac{\Gamma(K \rightarrow \pi \ell \nu(\gamma))}{\Gamma(\pi^+ \rightarrow \pi^0 e^+ \nu(\gamma))} = 1.9884(115)_{\pi}(93)_K \times 10^7, \quad (4)$$

when combined with $K_{\ell 3}$ decays. As shown in Fig. 1, this would match the precision of the current extraction of $|V_{us}/V_{ud}|$ from the axial channels [50] via

$$R_A = \frac{\Gamma(K \rightarrow \mu \nu(\gamma))}{\Gamma(\pi \rightarrow \mu \nu(\gamma))} = 1.3367(25), \quad (5)$$

thus providing a new competitive constraint on the $|V_{us}|-|V_{ud}|$ plane and probing NP that might affect vector and axial-vector channels in different ways. In the second step, an order of magnitude improvement in the BRPB precision will be sought in PIONEER Phase III program. This would provide the theoretically cleanest extraction of $|V_{ud}|$ at the 0.02% level, comparable to the current value from superallowed beta decays [51].

Finally, PIONEER will improve sensitivity to a host of exotic decays, including probes for the effects of heavy neutrinos [2, 6–8, 52–60], unique capabilities to search for pion decays to various light dark sector particles [8, 61–63], and lepton-flavor-violating decays of the muon into light NP particles $\mu \rightarrow eX$.

IV. PIONEER EXPERIMENT

A. Experiment Overview and Strategy

The main challenge in developing a next generation experiment for a high precision measurement of rare pion decays is accurately assessing the performance of the chosen detector technology in suppressing sources of systematic uncertainties and handling increased rates. The PIONEER detector design concept is based on the experience gathered with the PIENU [2] and PEN/PiBeta [49, 64, 65] experiments. Generically, the detector will have the features sketched out in Fig. 2.

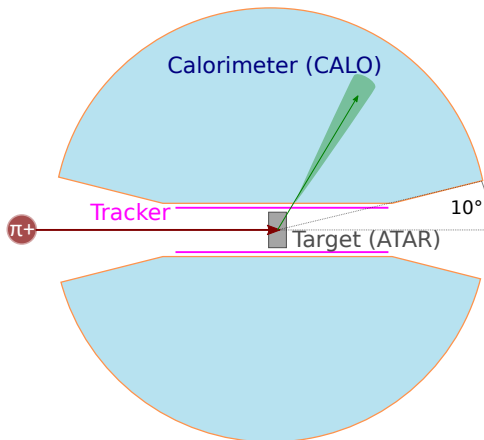


FIG. 2 – Layout of the PIONEER rare pion decay experiment. The intense positive pion beam enters from the left and is brought to rest in a highly segmented active target (ATAR). Decay positron trajectories are measured from the ATAR to an outer electromagnetic calorimeter (CALO) through a tracker. The CALO records the positron energy, time and location.

An intense pion beam is brought to rest in an instrumented (active) target (ATAR) and an electromagnetic calorimeter (CALO) surrounds the stopping target. A cylindrical

tracker surrounding the ATAR is used to link the locations of pions stopping in the target to showers in the calorimeter. Features of the PIONEER approach will include improved time and energy resolutions, greatly increased calorimeter depth, high-speed detector and electronic response, large solid angle coverage, and complete event reconstruction. The proposed detector will include a 3π sr, 25 radiation length (X_0) electromagnetic calorimeter, an advanced design segmented stopping target, and beam and positron trackers.

Phase I of PIONEER aims to measure $R_{e/\mu}$ with precision of 0.01%, where the uncertainty budget is equally allocated to statistics and systematics; 2×10^8 $\pi^+ \rightarrow e^+\nu$ events are required. Future phases will focus on a 3-fold (10-fold) improvement in the measurement of the ultra-rare pion beta decay process, $\pi^+ \rightarrow \pi^0 e^+\nu$. The $\pi^+ \rightarrow \pi^0 e^+\nu$ branching ratio is 10^4 times smaller than the $\pi \rightarrow e\nu$ channel and will require running with a 100x more intense pion flux. The event identification is more straightforward owing to the characteristic signature of the $\pi^0 \rightarrow \gamma\gamma$ decay in the calorimeter. While the optimization of the beam properties, instrumentation, and stopping target details for the pion beta decay experiment may require replacements of some systems, the core calorimeter, mechanics, tracker, and DAQ systems will be designed to meet the needs of both experiments with limited modifications.

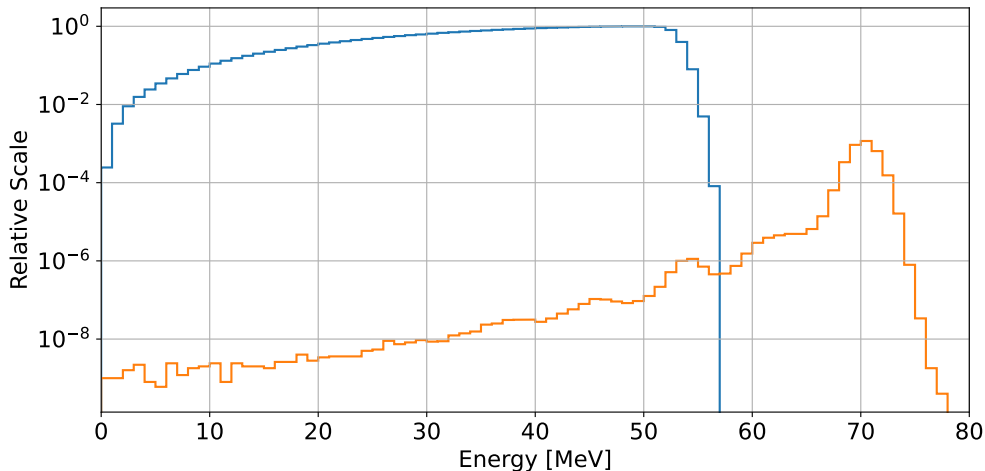


FIG. 3 – The positron energy spectra from muon decays (blue) and from $\pi \rightarrow e\nu$ decays (orange) for a calorimeter resolution of 1.5% and a depth of $25 X_0$. The simulation includes energy losses owing to photonuclear interactions.

At rest, the pion lifetime is 26 ns and the muon lifetime is 2197 ns. The monoenergetic positron from $\pi \rightarrow e\nu$ has an energy of 69.3 MeV. Positrons from ordinary muon decay form the Michel spectrum from 0 to an endpoint of 52.3 MeV. In principle, the monoenergetic e^+ from $\pi \rightarrow e\nu$ is well isolated above the Michel endpoint and can be easily identified using a high-resolution, hermetic calorimeter. To determine $R_{e/\mu}$ we measure the ratio of positrons emitted from $\pi \rightarrow e\nu$ and $\pi \rightarrow \mu \rightarrow e$ decays for which many systematic effects such as solid angle acceptance cancel to first order. However, counting all $\pi \rightarrow e$ events with a precision of one part in 10^4 requires determining the low-energy tail of the electromagnetic

shower and radiative decays that hide under the Michel spectrum from the $\pi \rightarrow \mu \rightarrow e$ chain, which has four orders of magnitude higher rate.

Figure 3 illustrates the relationship between the two channels and their respective positron energy spectra. Here, we have modeled the spectrum from both channels assuming a high resolution, $25 X_0$ calorimeter. There remains an unavoidable tail fraction below 53 MeV that must be determined accurately in order to obtain the branching ratio. That challenge was critical to previous generations of experiments and was responsible for the leading systematic uncertainty in the PIENU experiment at TRIUMF. PIONEER will minimize the intrinsic tail fraction through the use of a $25 X_0$ LXe calorimeter, the design of which is based on the considerable experience of the MEG Collaboration[66].

It is also important to be able to create triggers that can isolate $\pi \rightarrow e$ from $\pi \rightarrow \mu \rightarrow e$ chains within the stopping target, identify pion and muon decays in flight, as well as identify pileup from long-lived muons remaining in the target from earlier pion stops. To distinguish event types, we will use an active target that can provide 4D tracking (at the level of $150 \mu\text{m}$ in space and $<1 \text{ ns}$ in time) and energy measurements from the $O(30)$ keV signals for positrons to the 4000 keV Bragg peaks of stopping pions and muons. New low gain avalanche detector (LGAD) sensors have been identified as meeting these requirements. Simulation studies show that, by combining information from the active target and the calorimeter, $\mu - e$ backgrounds in the tail region can be suppressed to a level such that uncertainty in the tail fraction contributes $< 0.01\%$ to the error in $R_{e/\mu}$.

In Phase II (III), pion beta decay $\pi^+ \rightarrow \pi^0 e^+ \nu$ will be measured by observing the characteristic (nearly) back-to-back gammas from π^0 decay normalized to $\pi \rightarrow e \nu$ decay as in [43–47]. In PIONEER, it is also possible to observe the low-energy positron absorbed in the ATAR in coincidence with the gammas in the calorimeter. The Phase II (III) pion beta decay experiment will require 7×10^5 (7×10^6) events at an intrinsic branching ratio of 10^{-8} . This will require running at a significantly higher pion flux of $\geq 10 \text{ MHz}$. The beam momentum and emittance may be higher than for the $\pi \rightarrow e \nu$ measurement to achieve the higher flux.

B. Conceptual Design

The previous section described a generic PIONEER design in Fig. 2 and described the motivation for certain design choices. Figure 4 shows a more specific conceptual design, which includes the beamline and beamline instrumentation, the ATAR, a cylindrical tracker surrounding the ATAR, and a liquid xenon (LXe) calorimeter. An alternative calorimeter based on LYSO crystals, which provides natural segmentation, is also being investigated as an alternative to LXe. In this section, each component of this conceptual design is briefly described and opportunities for detector innovation and R&D are identified. More detail is available in [9].

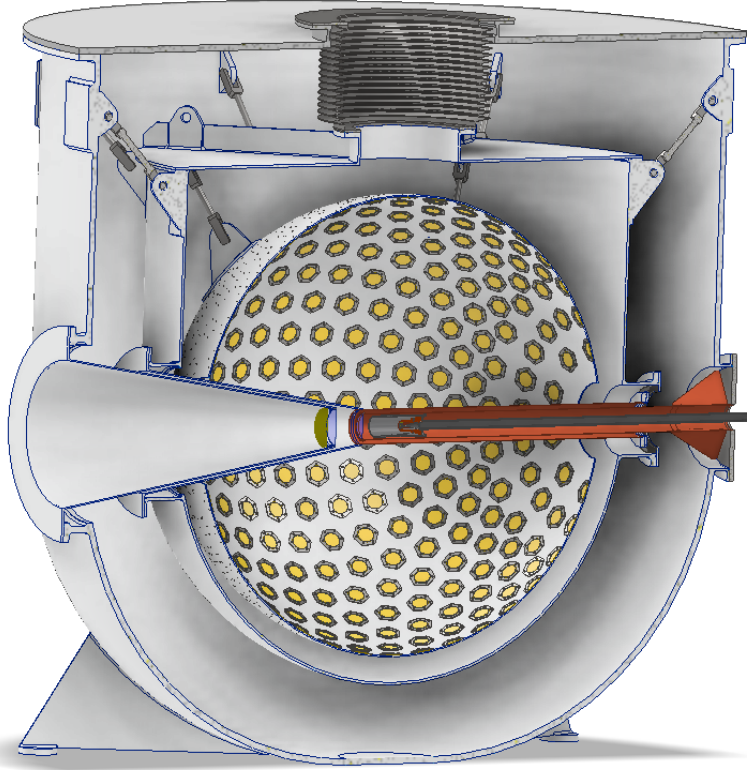


FIG. 4 – PIONEER conceptual design. The sphere is a LXe calorimeter, with the beam entering from the left, and the ATAR at the center. For scale, the lid is 3.05 m diameter. The yellow circles are merely representative of the LXe photosensors; they are not placed accurately.

1. Beam

The experiment will require a continuous wave low-momentum pion beam that can be focused to a small spot size and stop within the ATAR dimensions. Ideal characteristics include a relatively low momentum of $55 \text{ MeV}/c$ ($\pm 2\%$) and a flux of 300 kHz . At this low momentum, a separator is very effective to reduce background from beamline muons and positrons. The required beam properties are summarized in Table I and can be provided by the $\pi E5$ beam at PSI, which is a high-intensity low-energy muon and pion beamline, with a maximum momentum of $120 \text{ MeV}/c$, that is used for particle physics experiments, and is currently home to the MEG II and Mu3e experiments. Simulations for both pion production and transport of particles down the $\pi E5$ channel were performed using the G4Beamline toolkit [67]. Pion rates calculated in the simulation at the center of the calorimeter, for a 2% momentum bite, are sufficient for the $R_{e/\mu}$ measurement planned in Phase I of PIONEER, even when further losses due to collimation necessary for reducing background events in the ATAR and calorimeter are included. For PIONEER Phase II, III increasing the momentum and the momentum bite will be required.

Phase	p (MeV/c)	$\Delta p/p$ (%)	ΔZ (mm)	$\Delta X \times \Delta Y$ (mm ²)	$\Delta X', \Delta Y'$	R_π (10 ⁶ /s)
I	55-70	2	1	10x10	$\pm 10^\circ$	0.3
II,III	≈ 85	≤ 5	3	15x15	$\pm 10^\circ$	20

TABLE I – Required beam properties. ΔZ and $\Delta X \times \Delta Y$ are longitudinal (FWHM) range width and transverse (FWHM) beam sizes at target location, respectively.

2. Active Target

A highly segmented active target (ATAR) [68] is a key new feature of the proposed PIONEER experiment. Relative to previous experiments, the use of ATAR allows for discrimination against backgrounds by looking for deposition patterns internal to the target that are associated with the various signals' decay topologies. The ATAR will define the fiducial pion stop region, provide high resolution timing information, and will furnish selective event triggers. Examples of simulated ATAR event displays for $\pi \rightarrow e\nu$ and $\pi \rightarrow \mu \rightarrow e$ events are shown in Fig. 5.

To adequately suppress background from $\pi \rightarrow \mu \rightarrow e$ decay at rest (π DAR), pion and muon decay-in-flight (DIF), and accidental muon stops that precede the trigger signal, the ATAR must be able to detect both the exiting e^+ , a minimum ionizing particle (MIP), and larger (~ 100 MIPs) energy deposits from π^+ and μ^+ . The large dynamic range $O(2000)$ of the signals is a significant challenge for the readout electronics in the amplification and digitization stages. The position of the energy deposits needs to be identified with sufficient granularity along the beam direction and in the transverse plane. Furthermore, to identify single components of the decay processes a ~ 1.5 ns pulse pair resolution is needed.

The chosen technology for the ATAR is Low Gain Avalanche Detector (LGAD) [69], thin silicon detectors with moderate internal gain; the LGAD technology was chosen over standard silicon technology because of the intrinsic gain and thin bulk. A 120 μm thick LGAD sensor, coupled to fast electronics, has a time resolution of less than 100 ps on the rising edge and can separate a single hit from two overlapping hits if they arrive more than 1.5 ns apart. There are two specific LGAD technology options under consideration. The first option, AC-LGADs, overcome the granularity limitation of traditional LGADs and have been shown to provide spatial resolution of the order of tens of μm [70]. AC-LGAD design also allows to have a completely active sensor with no dead regions. The second option is Trench Isolated (TI) LGADs, which are a novel silicon sensor technology that utilizes a deep narrow trench to electrically isolate neighboring pixels to prevent breakdown, as opposed to standard LGADs which use a junction termination extension to prevent breakdown at the pixel edges [71]. By utilizing the deep trench isolation technology, the no-gain region is reduced to a few micrometers, thus achieving a higher fill factor than regular LGADs.

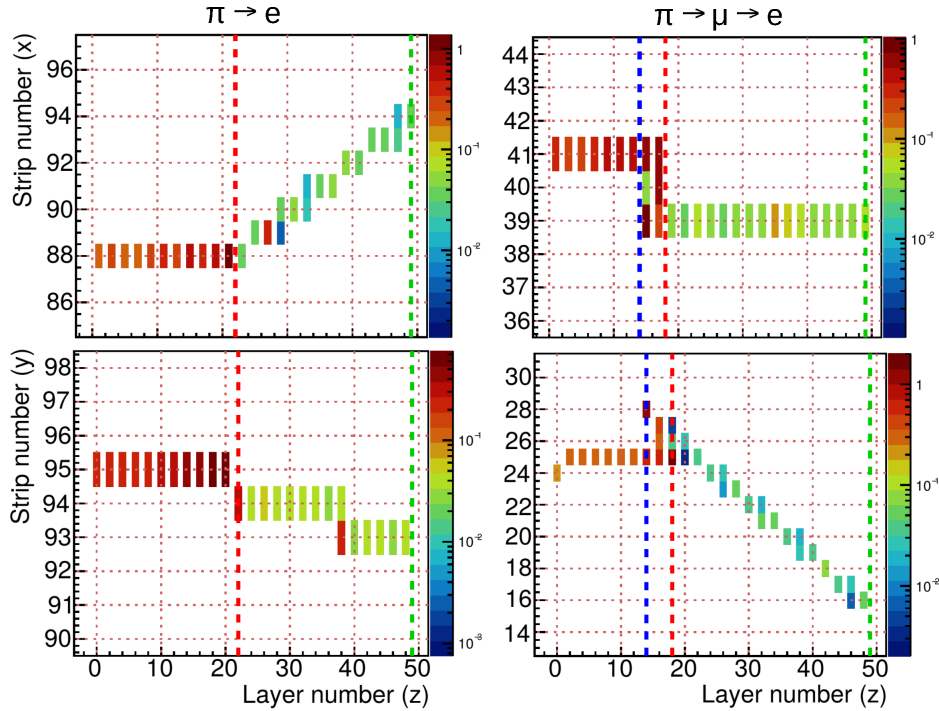


FIG. 5 – Simulated example displays of pion decay events in the ATAR. Pions enter horizontally from the left; the red dotted lines show the positions of the pion stops. The color of the bars indicates the deposited energy. Left column: X-Z (top) and Y-Z (bottom) strip views of a $\pi \rightarrow e\nu$ event. Right column: Same views of a $\pi \rightarrow \mu \rightarrow e$ event. The blue dotted line shows the position of the decay muon stop.

A preliminary design for the ATAR is shown in Fig. 6. In this design, the ATAR dimensions are $2 \times 2 \text{ cm}^2$ transverse to the beam. In the beam direction individual silicon sensors are tightly stacked with a total thickness of $\sim 6 \text{ mm}$. The detector is arranged in a strip geometry, with the strips oriented at 90° to each other in subsequent staggered planes to provide measurement of both coordinates of interest, and with the electronic readout connected on the side of the active region via wire bonding. The sensor geometry has strips with a pitch of $200 \mu\text{m}$, so that a sensor would have 100 strips mated to a chip with 100 channels and 2 cm width, a standard dimension for microchips. Sensor thickness is around $120 \mu\text{m}$, such that ~ 50 planes are needed to reach a total thickness of about 6 mm . The detectors are paired with the high-voltage facing each other in a pair to avoid ground and high voltage in proximity and the strips are wire bonded, with a connection alternating on the four sides, to a flex that brings the signal to a readout chip positioned a few cm away from the active volume. Readout from both ends is being investigated to reduce the average material traversed by exiting positrons; in the single-sided readout design, the maximum material in the path of the positrons occurs when 12 flexes are traversed.

R&D and optimization of the ATAR design is ongoing. Preliminary LGAD studies done

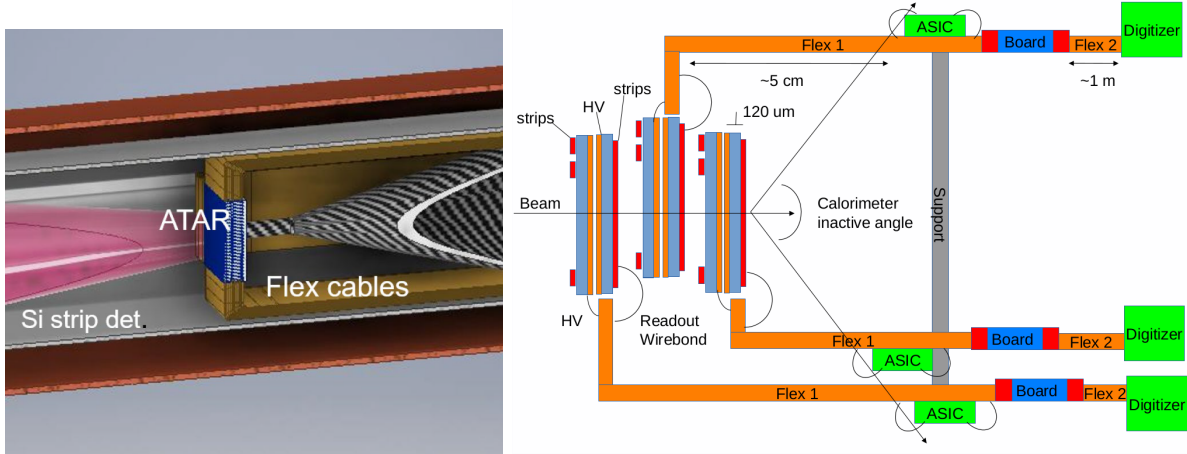


FIG. 6 – Left: ATAR position in the beam line. Right: Concept schematic design of the ATAR. The flex from the first, third and fifth sensors is directed in and out of the page. The modules are attached on the HV side and with a few μm of separation on the strip side. 48 sensors are coupled in 24 pairs.

with X-rays coming from the Stanford light source (SSRL) [72] and PSI [73] show that LGADs have an energy resolution of around 10%. The effect of gain saturation that was reported in the community in the past year [74] also needs to be studied. Strip AC-LGAD prototypes from Brookhaven National Lab (BNL) have been tested with a laboratory IR laser TCT station [75] and at a Fermilab (FNAL) test beam [76]; the position resolution of this prototype sensor varies between 5-15 μm in the direction perpendicular to the strip. Prototypes TI-LGADs sensors from Fondazione Bruno Kessler (FBK) [71] were studied at UCSC and found to have the standard response of a conventional LGAD with a small amount of “cross-talk” constant response of the sensor along the strip. In the next few years, several prototypes will be tested in laboratories and test beams to identify an optimized LGAD configuration for PIONEER.

The amplifier ASIC to read out the ATAR needs to be fast enough for the sensor in use; for the signal rise time in the 120 μm -thick prototype sensors, a bandwidth of 1 GHz should be sufficient. However, the high dynamic range (2000) requirement for the ATAR brings major complications to the readout. Current fast readout chips usually have a dynamic range of < 1000 , since they are targeted at MIPs-only detection in tracker sub-systems. One possibility is to develop an amplifier chip with logarithmic response or dynamic gain switching as well as a high enough bandwidth, currently no such chip exists with the necessary characteristics. Already available integrated chips, such as FAST [77] and FAST2, are being evaluated. Some new ASIC technologies that are being developed at UCSC in collaboration with external companies can run with 2.5V maximum signal, this allows for an increased dynamic range.

To successfully reconstruct the decay chains, the ATAR is expected to be fully digitized

at each event. To achieve this goal, a high bandwidth digitizer with sufficient bandwidth and sampling rate have to be identified. The same issue afflicting the amplifier, the high dynamic range, is also problematic for the digitization stage. A digitizer that would suit PIONEER’s requirements needs to be identified; a ready commercial solution would be the best option but the cost per channel might be prohibitive. For this reason the collaboration is exploring the possibility to develop a new kind of digitizer specific to this application.

3. *Cylindrical Tracker*

A dual layer cylindrical silicon strip tracker is situated between the ATAR and the calorimeter to measure the positron position in two dimensions (along the beam direction, z , and azimuthal angle, ϕ), and time. The detector has an inner diameter of 5 cm and a length of 25 cm. Overlapping lengths of long strips (about 10 cm) are needed to cover the entire region. Two layers of strips with a small stereo angle between them will provide O(mm) z resolution and 300 μm resolution in the direction perpendicular to the strips. An alternative under consideration is to connect two or three strip sensors in a line reading out both ends to obtain O(mm) position information along the strip position using charge attenuation information. The silicon strip sensors may be constructed with either regular silicon or LGADs.

4. *Liquid Xenon Calorimeter*

Due to its fast timing properties, high light yield with excellent energy resolution and highly uniform response, liquid xenon (LXe) read out by UV sensitive phototubes and state-of-the-art vacuum ultraviolet (VUV) silicon photomultiplier (SiPMs) is considered for the calorimeter. Here, experience is drawn from the MEG [78] and MEG-II [79] experiments which use a large scale, high rate LXe detector to search for the lepton flavor violating muon decay, $\mu^+ \rightarrow e^+\gamma$. Experiments searching for elusive dark matter (e.g. XENON, LUX-ZEPLIN) and (neutrinoless) double beta decay events (KamLAND-Zen, (n)EXO) also use detectors with similar scale liquid xenon cryostats. PIONEER, like MEG, detects only scintillation light (other experiments rely on both scintillation and charge collection) and is a high rate experiment. The PIONEER LXe detector is foreseen to be a 25 radiation length, 3π -sr sphere surrounding the ATAR.

The homogeneity of the LXe detector is an advantage in achieving the high energy resolution which is important for determining accurately the low energy “tail” fraction of $\pi \rightarrow e\nu$ events. MEG currently reports an energy resolution of $\sigma = 1.8\%$ for 50 MeV gammas and they continue to study possible improvements. The baseline energy resolution goal for PIONEER at 70 MeV is 1.5%.

The energy resolution is impacted by the efficiency of collection of scintillation light

which is itself influenced by design parameters (like photo-sensor coverage) and physical or technical parameters (like the light attenuation due to impurities in LXe, reflection of VUV light on surfaces, photo sensor refraction index, the level of dark current which impact the photo-electron threshold for summing the energies of the different photo-sensors, etc). In addition to the finite energy resolution of the calorimeter, photo-nuclear interactions, shower leakage and geometrical acceptance contribute to the low energy tail. The impact of photo-nuclear effects in LXe, for which little literature exists, will be determined by simulation and bench-marked against available data and new measurements.

A GEANT-4 simulation of a bare LXe calorimeter geometry was used to determine the residual tail fraction below the Michel end point versus calorimeter depth for $\pi \rightarrow e\nu$ events. Figure 7, Left, shows the energy deposited in the spherical calorimeter vs. the angle Theta with respect to the beam axis for a $25 X_0$ calorimeter depth. Figure 7, Right, shows the fraction of the energy deposited that is below 58 MeV vs. depth. The volume of LXe required scales as the radius cubed and the required photo-sensor coverage scales as the radius squared. These practical factors are optimized for smaller depth. The containment of the shower slowly improves with increased depth. This choice, along with the spherical shape and optimization of the calorimeter geometrical parameters and assessment of the expected detector sensitivity is ongoing.

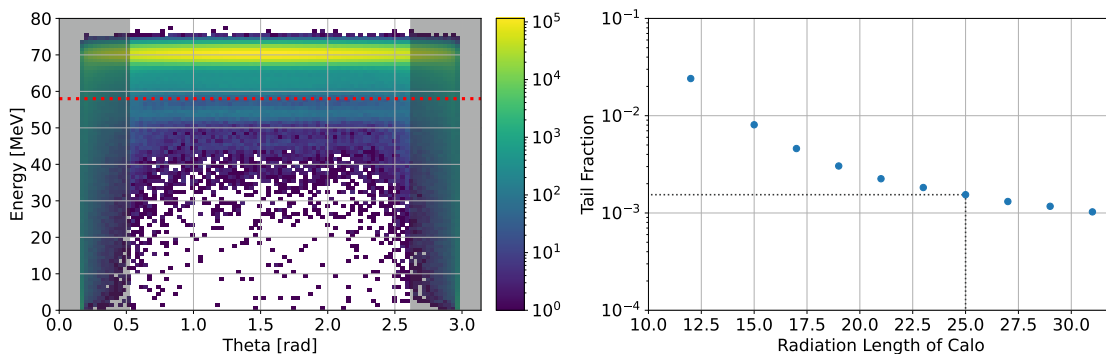


FIG. 7 – Left: The energy deposited by monoenergetic 69.3 MeV e^+ from $\pi \rightarrow e\nu$ decays in a $25 X_0$ calorimeter with an energy resolution of 1.5% vs. the angle Theta with respect to the beam axis. The grey bands indicate the boundaries of the fiducial volume region (here, 30°). Right: The shower tail fraction below 58 MeV vs. the calorimeter depth in radiation lengths for the 69.3 MeV $\pi \rightarrow e\nu$ events.

In order to readout the liquid xenon scintillation light, special photo sensors are necessary due to the short scintillation wavelength of 175 nm and the low operation temperature of 165 K. Two types of photo sensors were developed for this purpose by Hamamatsu K.K. and the MEG/MEG II collaboration: 2-inch photomultipliers (PMT) and multi-pixel photo sensors (MPPC). A round-shaped 2-inch PMT sensitive to VUV light (R9869) achieved a quantum efficiency of 15 %. The gain of the PMTs was found to decrease due to damage to the dynode induced by photoelectrons; however the PMT lifetime is sufficiently long to not

be of concern for PIONEER. In order to improve the granularity for the inner surface in the MEG-II experiment, a silicon photomultiplier, with an active area of $12 \times 12 \text{ mm}^2$, was developed. There are several advantages, in addition to higher granularity, to using SiPMs with respect to photomultiplier tubes: they are insensitive to magnetic fields, the single photoelectron peak can be used for calibration of the sensor, and the required supply voltage is relatively low (less than 100 V). However, while the MEG-II collaboration reported a photon detection efficiency (PDE) of $\sim 20\%$ [79], they observed later degradation of the PDE in LXe [80] which is under investigation. For this reason, the baseline design for PIONEER is the use of PMTs on the outer surface targeting a coverage of 20% (1000 phototubes) of the surface. The choice of photosensor technology may evolve depending on the developments regarding SiPM performance degradation.

The digitization and readout electronics proposed for the calorimeter are shown in Fig. 8. The 12 channel digitization boards will utilize the Analog Devices AD 9234 dual channel, 12 bit 1 giga-samples per second (GSPS) ADC chip, chosen for its low latency of 59 ns from presentation of the signal at the front end to output of the digitized signal. Calorimeter information can be summed with a pipelined adder and potentially corrected with a running pedestal measurement as the first stage in a total energy measurement. By clocking the ADC at the slightly lower rate of 976 MHz, the ADC information can be synchronized to the firefly data transfer rate of 244 MHz, simplifying synchronization of the system. The ADCs will sample continuously with samples stored initially in a ring buffer on the FPGA. Upon receipt of a trigger, a configurable time window will be stored in DIMM memory. By deploying a DIMM with a 128 bit data path, simultaneous reading and writing can be accomplished via two 64 bit pathways. A single FPGA will control one pair of ADCs (four calorimeter channels). It can compare the energy sum from each channel against a channel activity threshold (or thresholds), as well as combine the four running energy sums as the first stage of a total energy sum for the high energy trigger. That FPGA will also drive a single firefly channel. The digitizer boards will communicate with intermediate Apollo boards via the 16.1 GHz firefly links, which come packaged with a minimum of four individual links. Three of these links will provide the TCDS (or equivalent) clock and control signals and send the trigger and channel readout information to each of three sets of 4 ADC channels. The fourth firefly line will provide PCIe or Ethernet communication to allow board configuration and other slow control functions.

The xenon scintillation light absorption length has been measured for MEG to be more than 1 m [81]. However, the light absorption length can be significantly reduced through absorption by impurities such as H_2O and O_2 . A large scale detector requires purification at the ppb level which was achieved by MEG. The purification system and the cryostat design (needed to maintain the xenon at 165 K [66]) of MEG will be considered for scaling up the design for PIONEER. Details of the cryogenics, purification, and mechanical engineering have been considered and are described in more detail in [9].

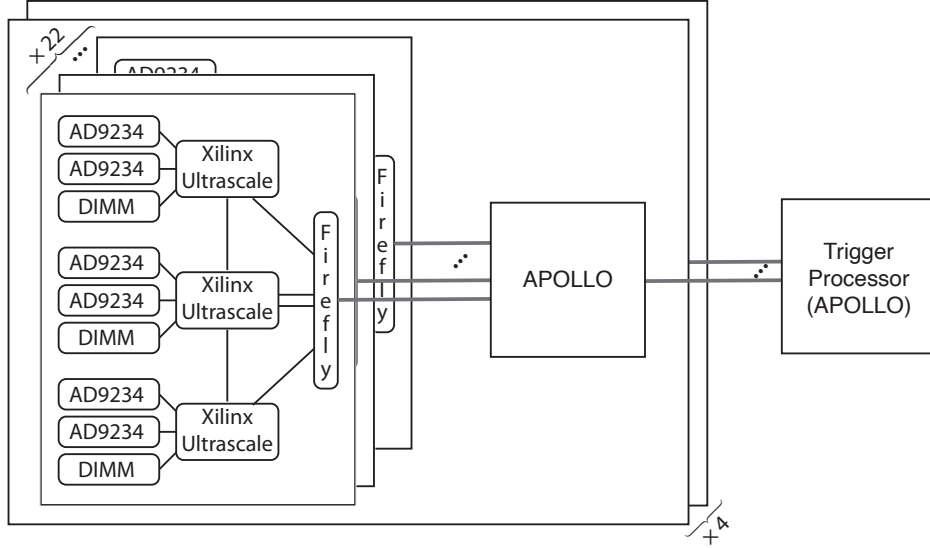


FIG. 8 – Proposed calorimeter digitization and readout. The 12 channel digitizer boards utilize the dual channel AD9234 12 bit, 1 GSPS ADCs, Xilinx Ultrascale FPGAs for control, and Samtec Firefly™ high speed communications to a CMS APOLLO board. The APOLLO board can receive up to 22 boards in this configuration – instrumenting quadrant of an order 1000 channel calorimeter.

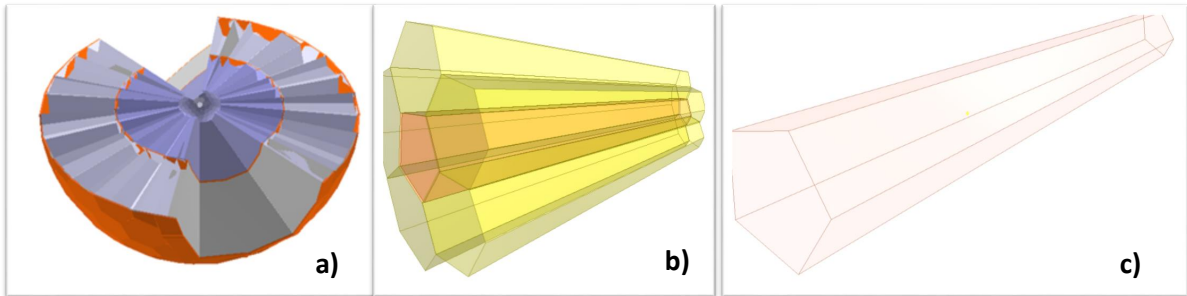


FIG. 9 – Possible use of an inner array of tapered LYSO crystals within the open volume of the existing PEN CsI calorimeter. a) Opened view showing in blue the array of LYSO crystals that matches one-to-one to the existing geometry of the PEN crystals shaded in gray. b) An example array ideal for testing the concept. c) An individual pentagonal crystal, $16X_0$ in depth. Each such crystal would be read out by a thin array of SiPMs.

5. Considerations on the Alternative LYSO Calorimeter

A naturally segmented array of tapered LYSO crystals provides an attractive alternative to our proposed LXe-based calorimeter. As shown in Fig. 9a, we are exploring a geometry that matches that of the PEN pure CsI detector [44–47, 64]. An inner array of LYSO crystals, a Cerium doped Lutetium based scintillator, can be inserted between the ATAR

and the existing PEN CsI array. Figures 9b and c indicated prototype geometries that are designed to fit inside the PEN calorimeter. On this option, we have collected pros and cons as well as experiences of other groups from experts in the field [82]. LYSO is radiation hard, non-hygroscopic, and has high density ($X_0=1.14$ cm, $R_M=2.07$ cm) and a light yield comparable to the highly luminous NaI (Tl), but with much faster light signals. Its 420 nm typical scintillation light has a 40 ns single exponential decay time and the spectrum is well matched to conventional SiPM photosensors. On the other hand, the growth of relatively long LYSO crystals is a fairly new and expensive R&D effort, and the energy resolution may be a limitation based on existing tests [83]. In order to advance this alternative design, it is imperative to improve on the uniformity of light production and transmission along the length of the crystal [84]. We plan to perform R&D regarding the possibilities of using LYSO for PIONEER.

6. Trigger and Data Acquisition System

All triggers will start with a PI signal, which is a loose condition for an incident beam particle defined as a coincidence of the beam detectors upstream of the ATAR. The key point is that this trigger must not introduce any bias between $\pi \rightarrow e\nu$ and $\pi \rightarrow \mu \rightarrow e$ events. The main time distributions in the vicinity of the PI signal are sketched in Fig. 10. After an initial build-up with the pion lifetime, positron rates from $\pi \rightarrow \mu \rightarrow e$ reach their maximum before decreasing with the muon lifetime. The constant accidental rate from muon decays of other pions stopped in ATAR is high.

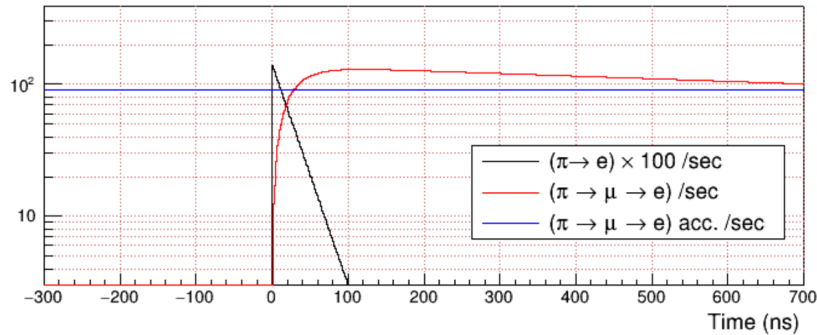


FIG. 10 – Positron rates after PI per second in 1 ns time bins. $\pi \rightarrow e\nu$ positron rates are multiplied by a factor 100. $\pi \rightarrow \mu \rightarrow e$ rates generated by PI shown in red and positron rates from old muons, i.e. from accidental pions, shown in blue.

After requiring the PI signal, several main triggers are formed, including a minimum bias trigger, with the PI signal prescaled by about $k=1000$, a trigger to select high energy ($E_{tot} \gtrsim 58$ MeV) events detected by the CALO within a time range $TR=[-300,700]$ ns relative to PI, a

trigger for all events with a TRACKER hit within time range TR relative to PI, prescaled by about $k=50$, and a trigger to select prompt events with a TRACKER hit in time range $[2,32]$ ns relative to PI, potentially prescaled. For all triggers, a full event readout, including the CALO waveforms, the ATAR and the BEAM and TRACKER detectors, will be initiated.

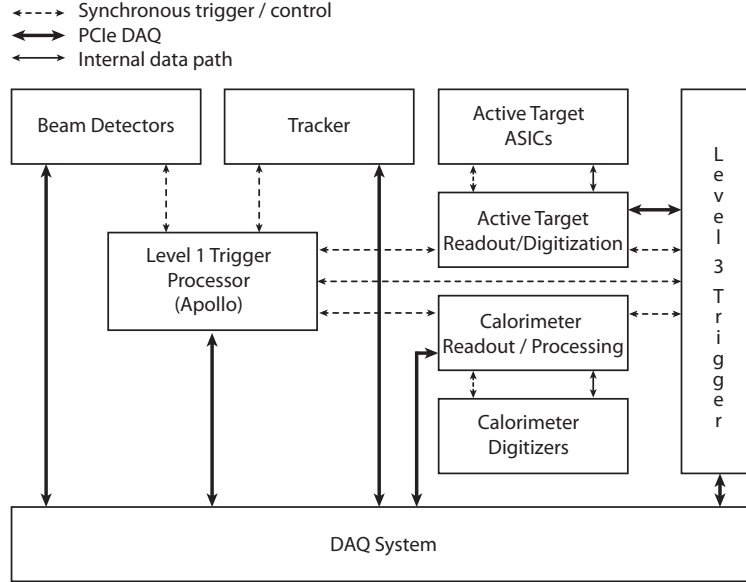


FIG. 11 – Proposed topology of the trigger and subdetector readout systems.

Figure 11 shows the planned topology for readout and triggering of PIONEER. The design takes advantage of the APOLLO [85] platform designed for the trigger track finder and pixel readout in the CMS experiment at the LHC. The platform supports flexible high speed synchronous command and triggering, as well as options for direct IO for receiving timing signals or generating trigger signals for devices expecting analog triggers. While by some measures this board likely provides more power than needed for PIONEER, it has already undergone significant prototyping with full production anticipated in 2024, and can satisfy several of the needs of the system with a single platform. The engineering group that designed the CM will also contribute to calorimetry readout, providing additional coherence.

The PIONEER data acquisition system must handle the readout, event assembly and data storage for the active target, positron tracker, electromagnetic calorimeter and other detector sub-systems of the experimental setup. It must provide a deadtime-free, distortion-free record of the datasets identified by the various physics and calibration triggers. It must facilitate the monitoring needed to guarantee the overall integrity of data taking and provide the metadata needed to document the experimental configuration during data taking. Finally, it must enable the configuration of the readout electronics and the associated trigger, clock and control system.

The acquisition will be implemented as a modular, distributed system on a parallel, layered processor array consisting of networked, multi-core, commodity PC's running an

operating system. The overall layout is depicted schematically in Fig. 12. It will comprise a frontend processor layer responsible for readout and processing of event fragments from the FPGA-based fast electronics instrumenting the various detector sub-systems, a backend layer responsible for event building and data storage, and an analysis responsible for monitoring of data integrity.

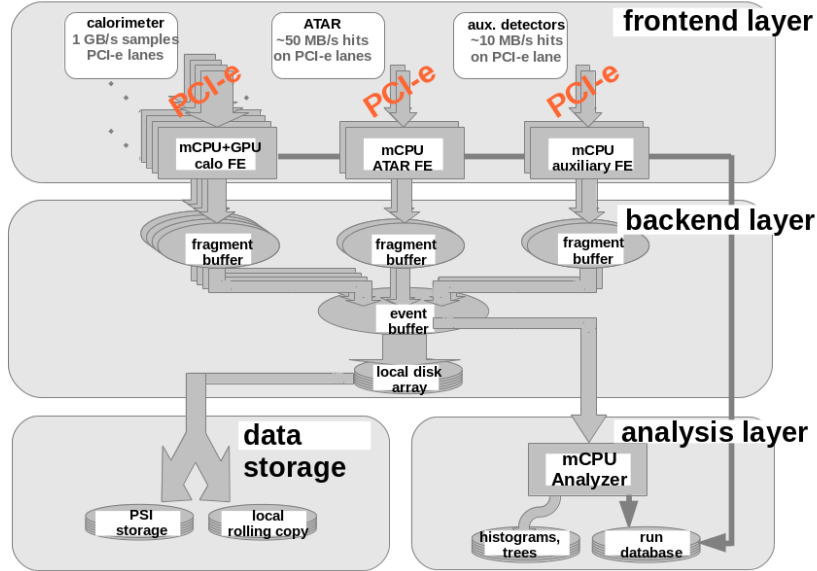


FIG. 12 – Schematic of the data acquisition system showing the frontend layer for data readout and experiment configuration, the backend layer for event assembly and data storage, and the analysis layer for data quality monitoring. The number of frontends and the topology of the FPGA-to-frontend and frontend-to-backend networks will be based on the calorimeter, ATAR and FPGA technology choices.

The DAQ software will be based on the MIDAS data acquisition package [86], CUDA GPU toolkit [87], ROOT data analysis package [88], and Linux PCI Express system and utility libraries. The MIDAS software consists of library functions for data flow between different processes on local / remote devices as well as infrastructure for data logging, experimental configuration and local /remote run control. It also incorporates an integrated alarm system and slow control system. The devices drivers for the configuration and the readout of the Apollo board FPGAs will be based on the PCI Express communication protocols / libraries.

The DAQ will process in real-time the data from a roughly 3.5 GB/sec raw data rate to a roughly ~300 MB/sec processed data rate for data storage on PSI’s Petabyte archive. One option for the data processing is the lossless compression of the slow decay-time calorimeter signals via a combination of delta encoding and Golomb coding. Other possibilities are zero

suppression of CALO islands and realtime fitting of CALO pulses. These algorithms are well suited to parallel processing using GPUs.

R&D is planned to demonstrate both the technology for the FPGA-to-CPU / GPU communication via optical PCI-express links and the performance of the data compression schemes. The conceptual design and R&D plan draw on experience with similar architectures of distributed data acquisition systems for the MuLan, MuCap and MuSun experiments at the PSI and the g-2 experiment at FNAL.

C. Simulations

Each of the design elements discussed above is being actively studied using GEANT4-based [89] simulations. The simulation efforts include beamline and upstream detector simulations, simulation of the active target, and simulation of the calorimeter. The $\pi E5$ beamline at PSI is simulated using G4Beamline [67]. The remainder of the simulation is done primarily using GEARS, an extension of GEANT4, which streamlines readout for rapidly iterating systems. The geometries for each of the experimental components are generated using a stand-alone Python script and geometry library, which takes as its input a `json` file of various parameters (e.g. diameters, number of elements, which detectors to implement, etc.) and exports a `GDML` file which is then read in by the Geant4 simulation. This file contains a full description of the physical geometry of the detectors, as well as their material properties (density, reflectivity, scintillation yield, etc.). Because of this workflow, it becomes trivial to implement scans over various parameters to perform systematic studies.

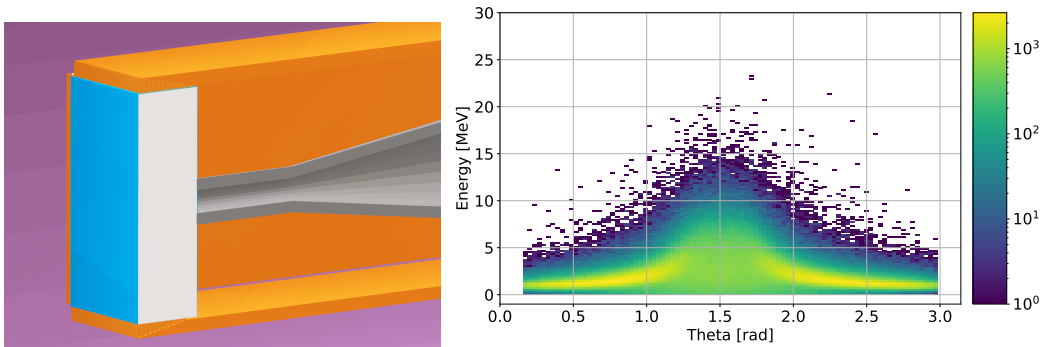


FIG. 13 – Left: An image of the simulated ATAR, showing the active planes (white) and readout strips (orange). Right: Total energy deposited in the ATAR by the decay positron as a function of the angle θ at which it enters the calorimeter.

1. ATAR Simulation

Simulations of the active target are done with both GEANT4, which allows us to model pions and their decay products through the full chain of detectors, and TRIM[90], which

allows us to track particle energy deposition precisely in a simulated detector readout. Figure 13 (left) shows the ATAR concept and (right) a simulation of energy deposit by exiting positrons as a function of polar angle of emission.

With an anticipated tail fraction $f = 0.5\%$ of $\pi \rightarrow e\nu$ events, $\mu - e$ decays must be suppressed to a level that allows measurement of $\Delta f/f$ with accuracy 1–2%. This can be accomplished by using ATAR information to identify stopped pions (and reject incoming muons) by energy loss, and range-energy relations, using a narrow time window (e.g. 3–35 ns) following the pion stop, rejecting events with observation of the 4.1 MeV decay muon, and suppressing events with pion decay-in-flight (π DIF), and muon decay-in-flight (μ DIF) following pion decay-at-rest (π DAR) by tracking and energy loss measurements. Experience from other experiments and PIONEER simulations indicate that $\pi \rightarrow \mu \rightarrow e$ background in the tail region from the dominant pion decay at rest will be suppressed to a negligible level, radiative decays $\pi \rightarrow \mu\nu\gamma$ followed by $\mu \rightarrow e$ decays which may leave < 4.1 MeV in the target will be suppressed by observation of the gamma and detection of the muon pulse and residual energy, and μ DIF can be suppressed to about 10% of the tail fraction f .

Another potentially significant low energy background in the tail region comes from π DIF in the ATAR followed by muon decay at rest. This component dominated the background suppressed spectrum in PIENU. Simulations indicate that 0.1% of pions decay in flight in the ATAR before stopping and initial studies indicate that the π DIF events can be suppressed by a factor of 5000 using ATAR tracking information which recognizes kinks in the topology and measures dE/dx along the track. Along with suppression of muon decays by selecting a narrow time window e.g. 3–35 ns after the pion stop, the estimated π DIF contribution to the uncertainty in the tail correction f is negligible.

There is an ongoing effort to apply machine learning tools to boost the sensitivity to $\pi^+ \rightarrow e^+\nu$ events in the tail region and suppress background. It has already been demonstrated with the in-ATAR π DIF events that gradient boosting decision trees (BDT) are able to outperform the manual cut-based methods. Although the BDT model shows excellent classification performance, there are further potential gains from deep neural networks, especially Convolutional Neural Networks (CNN), which have shown extraordinary performance in image processing and classification applications.

2. CALO Simulation

Simulation studies of the LXe calorimeter response have been performed using the GEANT4 package [89] with optical photon tracking. A simple geometry (see Fig. 14a) that is representative of the current design was implemented. $\pi \rightarrow \mu \rightarrow e$ events were generated in the target at the center of the LXe sphere and optical photons originating from LXe scintillation induced by the showers generated by the positrons were tracked until the outside sensitive surface of the LXe sphere. A pulse fitting algorithm was employed to evaluate

the possibility of separating events that overlap in time i.e. pulse pileup. Pulse separation down to 5 ns was achieved (see illustration in Fig. 14b) across a wide range of amplitudes. This gives a first indication (without digitization) of the performance of the detector and subsequent data analysis with respect to dealing with pileup.

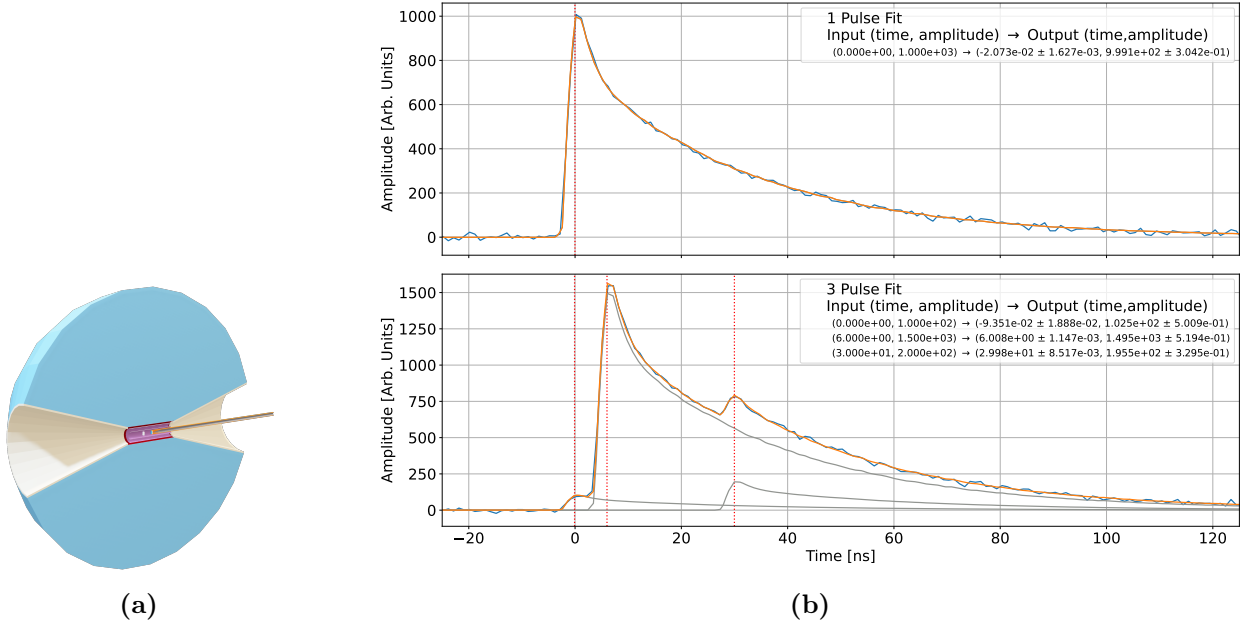


FIG. 14 – (a) Rendering of the simplified geometry used in the first Monte-Carlo simulation of the PIONEER LXe calorimeter (b) Example of simulated pulse shapes of a single $\pi \rightarrow \mu \rightarrow e$ event (top) and 3 events happening closely in time (bottom) and recorded in the LXe calorimeter. Pulse shape fitting based on a template allows accurate identification and energy reconstruction of multiple pulses down to ± 5 ns separation.

Further studies are anticipated to introduce and optimize optical qualities of the surfaces, optimize photo-sensing detector coverage, and improve the simulation of the originating scintillation photons. Much of the input for these simulations will be provided by test measurements. Position resolution will also augment pile-up handling capabilities. The position resolution capabilities of the detector and its importance for achieving the targeted rate will be modeled and studies are envisaged in the apparatus which will also be used to test the photo-sensors in LXe. Depending on the outcome of the pileup studies, segmentation of the LXe volume may be considered.

One important aspect of the calorimeter design that is being informed by the simulations is understanding how energy from a decay positron is ‘lost’ before it reaches the calorimeter. While energy lost in the ATAR is measured, losses occurring in inactive material e.g. the ATAR cabling, and calorimeter entrance windows, depend on the angle of emission. Simulations are being used to study these effects on the positron energy resolution.

Another important study involves modeling of photonuclear interactions. As decay

positrons interact with atomic nuclei in the simulation, they will occasionally cause a nucleus to enter into an excited state with single or multiple neutron emission. When these neutrons escape the calorimeter without depositing their energy the observed energy is shifted down by multiples of the neutron binding energy (see Fig. 3). Modeling and prototype studies will be pursued for evaluating these effects in LXe.

V. SENSITIVITY

The sensitivity of PIONEER has been evaluated using performance assumptions that are chosen to be compatible with the experimental conceptual design described above.

A. $\pi \rightarrow e\nu$

The first phase of PIONEER ($R_{e/\mu}$) will employ a beam with a pion stopping rate in the ATAR of approximately $3 \times 10^5/s$ at momentum of $55 - 70 \text{ MeV}/c$ with $\frac{\Delta p}{p} \leq 2\%$ in a spot size $\leq 2 \text{ cm}$ diameter. Muon and positron contaminations will be reduced to $< 10\%$ with the use of a separator as discussed above. To estimate the running time required to reach the proposed sensitivity, we assume that the beam will be available during 5 months per year. We also assume an overall event acceptance efficiency of 30%, which is based on the fiducial volume, the timing window cuts, and reconstruction factors. We assume a data-taking (operations) efficiency of 50% based on the product of PSI beam delivery and experimental data-collection uptime, along with an allocation for non-production systematic uncertainty tests. These factors result in $2 \times 10^8 \pi^+ \rightarrow e^+\nu$ events for a 3-year run satisfying the statistics goal.

Error Source	PIENU 2015 PIONEER Estimate	
	%	%
Statistics	0.19	0.007
Tail Correction	0.12	<0.01
t_0 Correction	0.05	<0.01
Muon DIF	0.05	0.005
Parameter Fitting	0.05	<0.01
Selection Cuts	0.04	<0.01
Acceptance Correction	0.03	0.003
Total Uncertainty	0.24	≤ 0.01

TABLE II – $Br(\pi \rightarrow e\nu)$ precision for PIENU 2015[2] (left) and estimated precision for PIONEER (right).

Systematic uncertainties for PIONEER have been estimated based on the experience of PIENU [2] and are shown in Table II. The main systematic uncertainty for PIENU was the uncertainty in the tail correction for $\pi \rightarrow e\nu$ events below 52 MeV. In PIONEER the tail will be reduced from 3% to 0.5% due to the increased thickness of the calorimeter ($25X_0$ compared to $\leq 19X_0$) and the more uniform acceptance due to the larger solid angle. The ATAR will allow suppression of π DIF and μ DIF backgrounds enabling more precise measurement of the tail. Uncertainties in the other small corrections, e.g. the pion stop time (t_0) Correction, Selection Cuts, and Acceptance Correction, are estimated to be reduced due to the improvements such as in the calorimeter and ATAR timing resolutions. An additional uncertainty arises from the pion lifetime, presently known to 0.02% precision [1]; the PIONEER group intends to make additional measurements to reduce this uncertainty to $< 0.01\%$.

B. Exotics

1. Massive neutrino searches $\pi^+ \rightarrow \ell^+ \nu_H$

Searches for peaks in the positron energy spectrum due to $\pi^+ \rightarrow \ell^+ \nu_H$ decays were performed in the PIENU experiment [59, 60] sensitive to masses $65 < m_H < 135$ MeV but no significant signal above statistical uncertainty was found. The measurement of $R_{e/\mu}$ [2] provides limits for $m_H < 65$ MeV. To estimate the expected sensitivities for PIONEER with $100\times$ the statistics (Phase I), reduced backgrounds, and improved detectors, toy MC simulations were performed.

For $\pi^+ \rightarrow e^+ \nu_H$ decays, the peak search sensitivity was limited by residual $\pi^+ \rightarrow \mu^+ \rightarrow e^+$ background from pion and muon decay-in-flight (π DIF and μ DIF). The low energy calorimeter response tail and statistics of the $\pi^+ \rightarrow e^+ \nu_e$ decay also limits the sensitivity. Using an active target and a larger electromagnetic calorimeter, the background $\pi^+ \rightarrow \mu^+ \rightarrow e^+$ will be significantly suppressed compared to PIENU, and a significantly smaller low energy $\pi^+ \rightarrow e^+ \nu_e$ tail is anticipated. Figure 15 shows the result of a toy MC study for the expected sensitivity (90% confidence level (C.L.) upper limits) in PIONEER, assuming 1×10^8 $\pi^+ \rightarrow e^+ \nu_e$ events, 1% tail fraction below 52 MeV, no $\pi^+ \rightarrow \mu^+ \rightarrow e^+$ events, improved energy resolution for decay positrons with respect to the PIENU calorimeter [91], and negligible acceptance corrections due to the larger detector acceptance. Compared with PIENU (red curves in the right panel in Fig. 15), the expected sensitivity in PIONEER would be improved by one order of magnitude.

The sensitivity for $\pi^+ \rightarrow \mu^+ \nu_H$ decay will also be improved by the larger PIONEER statistics. The dominant background is mainly due to the radiative pion decay $\pi^+ \rightarrow \mu^+ \nu_\mu \gamma$ with branching fraction 2×10^{-4} [92] (for $E_\gamma < 1$ MeV). A toy MC simulation was performed with 1×10^9 $\pi^+ \rightarrow \mu^+ \nu_\mu$ decays ($\times 100$ larger statistics than PIENU) including $\pi^+ \rightarrow \mu^+ \nu_\mu \gamma$

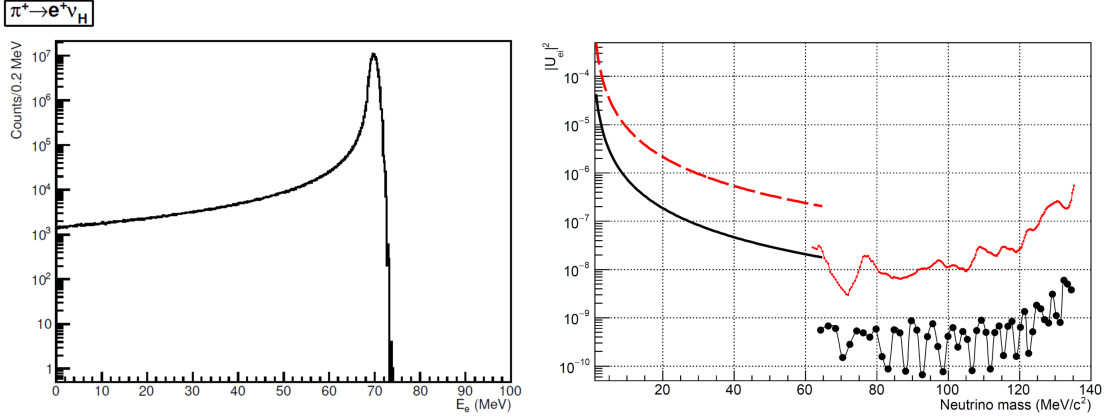


FIG. 15 – Left: simulated $\pi^+ \rightarrow e^+ \nu_e$ energy spectrum. Right: Limits on $|U_{ei}|^2$ (90% C.L.) from PIENU (red)[2, 59]) and expected sensitivity from PIONEER (black). The lower region limits ($m_H < 65$ MeV) come from the branching ratio measurement and the higher ($m_H > 65$ MeV) region from the peak search.

background considering the proper branching fraction, and assuming the same detector resolution as in PIENU. Figure 16 shows the results of the simulation and the PIENU experiment [60].

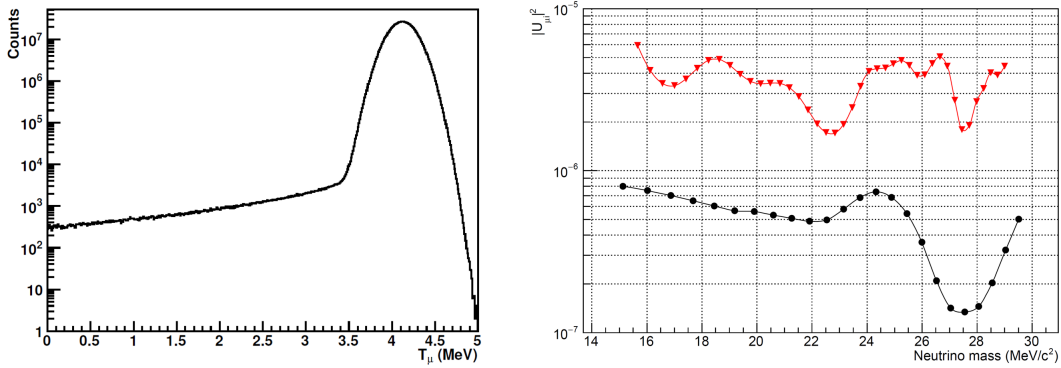


FIG. 16 – Left: simulated $\pi^+ \rightarrow \mu^+ \nu_\mu$ kinetic energy spectrum. Right: The PIENU result (red triangles [60]) and expected sensitivity with PIONEER (black circles) for the mixing matrix $|U_{\mu i}|^2$ (90% C.L. limit).

2. Two body muon decay $\mu^+ \rightarrow e^+ X_H$

Massive or massless weakly interacting neutral bosons X such as axions [93–96] and Majorons [97–99] have been suggested to extend the SM including models with dark matter candidates, baryogenesis, and solutions to the strong CP problem. Wilczek suggested a

model [100] which may lead to charged lepton flavor violation (CLFV) where the boson X can be emitted in flavor changing interactions.

When decay products from a massive boson X_H are not detected due to a long lifetime, flavor violating two-body muon decays involving a massive boson $\mu^+ \rightarrow e^+ X_H$ can be sought by searching for extra peaks in the Michel spectrum. This search was performed with PIENU, resulting in the limit to the branching ratio $\Gamma(\mu^+ \rightarrow e^+ X_H)/\Gamma(\mu^+ \rightarrow e^+ \nu \bar{\nu})$ at the level of 10^{-5} in mass range $47.8 - 95.1 \text{ MeV}/c^2$ [101]. The statistics will improve by two orders of magnitude with respect to PIENU.

To estimate the expected sensitivity, 2×10^{10} muon decays were simulated. Figure 17 shows the 90% C.L. upper limits of the branching ratio from different experiments and the expected sensitivity for PIONEER.

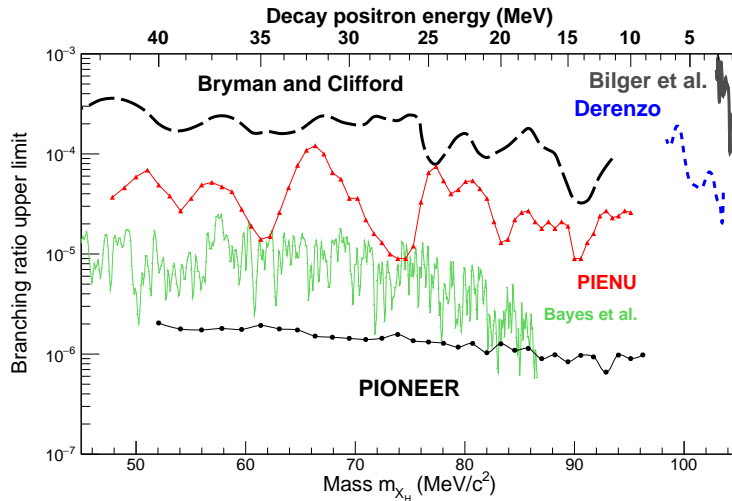


FIG. 17 – 90% C.L. limit of the branching ratio for PIONEER (black circles) and other past experiments (see Refs. [102–105] for more details).

3. Other decays

Three and four body pion decay modes can be analyzed with the same method as for the $\pi^+ \rightarrow \ell^+ \nu_H$ searches. However, the signal shapes in these cases are represented by continuous lepton energy spectra. The expected sensitivities will also be improved by one order of magnitude. The current limits set by the PIENU experiment are described below.

Three body pion decays $\pi^+ \rightarrow \ell^+ \nu X$, where X is a massive or massless weakly interacting particle, were searched for in the PIENU experiment [8]. The decay $\pi^+ \rightarrow e^+ \nu X$ was sought; no signal beyond the statistical uncertainty was observed, and 90% C.L. upper limits were set on the branching ratio $\Gamma(\pi^+ \rightarrow e^+ \nu X)/\Gamma(\pi^+ \rightarrow \mu^+ \nu)$ with $10^{-7} - 10^{-8}$ level in the mass range of $0 < m_X < 120 \text{ MeV}/c^2$.

The $\pi^+ \rightarrow \mu^+ \nu X$ decay was also searched for. A 90% C.L. upper limit was derived on

the branching ratio $\Gamma(\pi^+ \rightarrow \mu^+\nu X)/\Gamma(\pi^+ \rightarrow \mu^+\nu)$ at the $10^{-5} - 10^{-6}$ level in the mass region from 0 to 33.9 MeV/ c^2 .

The rare pion decays $\pi^+ \rightarrow \ell^+\nu_\ell\nu\bar{\nu}$ are highly suppressed. Thus, the experimental search for these processes could reveal small non-SM effects such as neutrino-neutrino interactions [106] and six-fermion interactions [107, 108], which might compete with the SM processes at first order. The rare pion decays, considering three models (SM, neutrino-neutrino interaction, and six-fermion) were also searched for in PIENU [109], and a first result for $\Gamma(\pi^+ \rightarrow \mu^+\nu_\mu\nu\bar{\nu})/\Gamma(\pi^+ \rightarrow \mu^+\nu_\mu) < 8.6 \times 10^{-6}$ and an improved measurement $\Gamma(\pi^+ \rightarrow e^+\nu_e\nu\bar{\nu})/\Gamma(\pi^+ \rightarrow \mu^+\nu_\mu) < 1.6 \times 10^{-7}$ were obtained.

C. Pion Beta Decay

For the $\pi^+ \rightarrow \pi^0 e^+ \nu$ experiment the positive pion stop rate would have to be higher, $\geq 10^7/s$, possibly with a larger momentum bite $\frac{\Delta p}{p} \approx 3\%$ and likely using higher pion momentum. This would result in 7×10^5 $\pi^+ \rightarrow \pi^0 e^+ \nu$ events collected for 4 years of (5 months/yr) operation assuming similar efficiency factors as discussed for the $\pi \rightarrow e\nu$ measurement.² This would be sufficient to achieve the required statistical precision to improve the pion beta decay branching ratio measurement precision by a factor of 3 (Phase II). Systematic effects are expected to be reduced to the 0.06% level (10× lower than for the previous PiBeta experiment) due to the combined improvements to the calorimetry (principally, the time and energy resolutions) and the ATAR which may facilitate the observation of the positron in $\pi^+ \rightarrow \pi^0 e^+ \nu$ decay in coincidence with the π^0 detection.

Running at higher rates may be possible leading to a further precision improvement of 3 (Phase III) and will depend on the ability of the spectrometer to deal with higher rates of pile-up of accidental events. In this regard, we are studying the possibility to optically segmenting the LXe volume.

VI. PLANNING FOR REALIZATION OF PIONEER

The PIONEER collaboration consists of participants from PIENU, PEN/PiBeta, and MEG/MEGII as well as experts in rare kaon decays, low-energy stopped muon experiments, the Muon $g - 2$ experimental campaign, high energy collider physics, neutrino physics, and other areas. The collaboration is still developing and welcomes new members.

The collaboration anticipates performing detector R&D in several areas, including the following:

- Beam studies will be preformed in $\pi E5$ (and possibly $\pi E1$) to establish the required beam conditions. Two weeks of beam time has been approved for 2022.

² In the Phase I measurement of $\pi \rightarrow e\nu$ PIONEER will collect a sizeable sample of pion beta decay events, which will be helpful to inform the Phase II (III) design.

- After initial sensor characterization and design optimization a PIONEER specific ATAR sensor prototype will be produced. The characterization includes studies on LGAD energy resolution and gain suppression mechanism.
- A first ATAR demonstrator with a few planes of available sensor prototypes will be produced. An electronics board with suitable characteristics needs to be designed and produced. The prototype would be then tested in a pion/muon beamline.
- Identification of suitable chips for the ATAR analog amplification and digitization.
- ATAR mock-ups: the support mechanics and thermal load will be studied with mock-up prototypes and silicon heaters.
- Cylindrical positron tracker. Designs with standard $300\ \mu\text{m}$ thick Si strips and with LGADs are being considered. We expect to construct and test prototypes of various geometries.
- LXe prototype: The objectives of this R&D work include determination of the properties of photo-sensors and optical properties of materials for use in the LXe calorimeter. We also want to benchmark the photon transport simulations. We are considering the development of a medium scale calorimeter prototype that would enable measurements of properties like energy resolution and photonuclear effects for validation of simulations.
- LXe calorimeter optical segmentation: Small prototypes will be used initially and UV compatible materials will be evaluated. Some of these studies may be done using a LXe cryostat at McGill university containing ~ 21 of LXe developed for SiPM tests for nEXO. An assembly hosting SiPMs, reflective material and a retractable radioactive source will be prepared at TRIUMF and brought to McGill for measurements.
- SiPMs: SiPM degradation at high rates will be studied. We will test available photosensors using small LXe prototypes in association with the McGill setup mentioned above.
- Crystal alternatives to LXe: Arrays of LYSO crystals with varying levels of doping will be evaluated from various manufacturers.
- DAQ: Rate testing of FPGA-to-CPU/GPU and CPU-to-CPU communication via optical PCI-express links will be done along with performance testing of data compression algorithms for CALO data.
- Trigger prototyping: A prototype APOLLO Command Module will be used. A 4-channel prototype of the digitizer board for evaluation and communications development will be built.

An optimistic schedule for PIONEER assuming that funding decisions are positive and proceed expeditiously, would allow an increasing amounts of prototype instrumentation on various sub systems (e.g. ATAR, DAQ) to be tested in the following years leading to the full-scale measurement program of Phase I to begin in 2029.

VII. SUMMARY

In this SNOWMASS white paper, the physics motivation and the conceptual design of a next-generation rare pion decay experiment, PIONEER, are described. Built upon the excellent 4D tracking capability of the LGAD-based active target and a large-acceptance, deep, fast, and uniform liquid Xenon calorimeter with excellent energy resolution, the Phase I PIONEER experiment, approved at PSI, aims at measuring the charged-pion branching ratio to electrons vs. muons $R_{e/\mu}$ at a precision of 1 part in 10^4 . This precise measurement of $R_{e/\mu}$ can be compared with the Standard Model (SM) prediction at similar precision to probe non-SM explanations of several experimental anomalies pointing towards the potential violation of lepton flavor universality through sensitivity to quantum effects of new particles up to the PeV mass scale. The later phases of the PIONEER experiment aim at improving the experimental precision of the branching ratio of pion beta decay, $\pi^+ \rightarrow \pi^0 e^+ \nu(\gamma)$, to test CKM unitarity and to extract $|V_{ud}|$ at the 0.02% level.

ACKNOWLEDGMENTS

This document was prepared by the PIONEER collaboration in coordination with scientific staff members at PSI. The members of the collaboration are supported by the U.S. Department of Energy, Office of Science, Offices of High Energy Physics and Nuclear Physics; the U.S. National Science Foundation; Natural Sciences and Engineering Research Council (Canada); TRIUMF; the Swiss National Science Foundation; and JSPS KAKENHI (Japan).

-
- [1] P. A. Zyla *et al.* (Particle Data Group), PTEP **2020**, 083C01 (2020).
 - [2] A. Aguilar-Arevalo *et al.* (PIENU), Phys. Rev. Lett. **115**, 071801 (2015), arXiv:1506.05845 [hep-ex].
 - [3] D. A. Bryman, M. S. Dixit, R. Dubois, J. A. Macdonald, T. Numao, B. Olaniyi, A. Olin, and J. M. Poutissou, Phys. Rev. D **33**, 1211 (1986).
 - [4] D. I. Britton *et al.*, Phys. Rev. D **49**, 28 (1994).
 - [5] G. Czapek *et al.*, Phys. Rev. Lett. **70**, 17 (1993).
 - [6] D. A. Bryman and R. Shrock, Phys. Rev. D **100**, 053006 (2019), arXiv:1904.06787 [hep-ph].
 - [7] D. A. Bryman and R. Shrock, Phys. Rev. D **100**, 073011 (2019), arXiv:1909.11198 [hep-ph].

- [8] A. Aguilar-Arevalo *et al.* (PIENU), Phys. Rev. D **103**, 052006 (2021), arXiv:2101.07381 [hep-ex].
- [9] W. Altmannshofer *et al.* (PIONEER), (2022), arXiv:2203.01981 [hep-ex].
- [10] A. Crivellin and M. Hoferichter, Science **374**, 1051 (2021), arXiv:2111.12739 [hep-ph].
- [11] O. Fischer *et al.*, (2021), arXiv:2109.06065 [hep-ph].
- [12] D. Bryman, V. Cirigliano, A. Crivellin, and G. Inguglia, (2021), arXiv:2111.05338 [hep-ph].
- [13] V. Cirigliano and I. Rosell, Phys. Rev. Lett. **99**, 231801 (2007), arXiv:0707.3439 [hep-ph].
- [14] D. Bryman, W. J. Marciano, R. Tschirhart, and T. Yamanaka, Ann. Rev. Nucl. Part. Sci. **61**, 331 (2011).
- [15] J. P. Lees *et al.* (BaBar), Phys. Rev. Lett. **109**, 101802 (2012), arXiv:1205.5442 [hep-ex].
- [16] R. Aaij *et al.* (LHCb), Phys. Rev. D **97**, 072013 (2018), arXiv:1711.02505 [hep-ex].
- [17] A. Abdesselam *et al.* (Belle), (2019), arXiv:1904.08794 [hep-ex].
- [18] R. Aaij *et al.* (LHCb), JHEP **08**, 055 (2017), arXiv:1705.05802 [hep-ex].
- [19] R. Aaij *et al.* (LHCb), Phys. Rev. Lett. **122**, 191801 (2019), arXiv:1903.09252 [hep-ex].
- [20] R. Aaij *et al.* (LHCb), (2021), arXiv:2103.11769 [hep-ex].
- [21] Y. S. Amhis *et al.* (HFLAV), Eur. Phys. J. C **81**, 226 (2021), arXiv:1909.12524 [hep-ex].
- [22] C. Murgui, A. Peñuelas, M. Jung, and A. Pich, JHEP **09**, 103 (2019), arXiv:1904.09311 [hep-ph].
- [23] R.-X. Shi, L.-S. Geng, B. Grinstein, S. Jäger, and J. Martin Camalich, JHEP **12**, 065 (2019), arXiv:1905.08498 [hep-ph].
- [24] M. Blanke, A. Crivellin, T. Kitahara, M. Moscati, U. Nierste, and I. Nišandžić, (2019), 10.1103/PhysRevD.100.035035, [Addendum: Phys. Rev. D **100**, 035035 (2019)], arXiv:1905.08253 [hep-ph].
- [25] S. Kumbhakar, A. K. Alok, D. Kumar, and S. U. Sankar, PoS **EPS-HEP2019**, 272 (2020), arXiv:1909.02840 [hep-ph].
- [26] M. Algueró, B. Capdevila, A. Crivellin, S. Descotes-Genon, P. Masjuan, J. Matias, M. Novoa Brunet, and J. Virto, Eur. Phys. J. C **79**, 714 (2019), [Addendum: Eur. Phys. J. C **80**, 511 (2020)], arXiv:1903.09578 [hep-ph].
- [27] J. Aebischer, W. Altmannshofer, D. Guadagnoli, M. Reboud, P. Stangl, and D. M. Straub, Eur. Phys. J. C **80**, 252 (2020), arXiv:1903.10434 [hep-ph].
- [28] M. Ciuchini, A. M. Coutinho, M. Fedele, E. Franco, A. Paul, L. Silvestrini, and M. Valli, Eur. Phys. J. C **79**, 719 (2019), arXiv:1903.09632 [hep-ph].
- [29] A. Arbey, T. Hurth, F. Mahmoudi, D. M. Santos, and S. Neshatpour, Phys. Rev. D **100**, 015045 (2019), arXiv:1904.08399 [hep-ph].
- [30] G. W. Bennett *et al.* (Muon $g - 2$), Phys. Rev. D **73**, 072003 (2006), arXiv:hep-ex/0602035.
- [31] B. Abi *et al.* (Muon $g - 2$), Phys. Rev. Lett. **126**, 141801 (2021), arXiv:2104.03281 [hep-ex].
- [32] T. Aoyama *et al.*, Phys. Rept. **887**, 1 (2020), arXiv:2006.04822 [hep-ph].

- [33] H. Davoudiasl and W. J. Marciano, *Phys. Rev. D* **98**, 075011 (2018), arXiv:1806.10252 [hep-ph].
- [34] A. Crivellin, M. Hoferichter, and P. Schmidt-Wellenburg, *Phys. Rev. D* **98**, 113002 (2018), arXiv:1807.11484 [hep-ph].
- [35] C. Bobeth, M. Bordone, N. Gubernari, M. Jung, and D. van Dyk, *Eur. Phys. J. C* **81**, 984 (2021), arXiv:2104.02094 [hep-ph].
- [36] A. Carvunis, A. Crivellin, D. Guadagnoli, and S. Gangal, (2021), arXiv:2106.09610 [hep-ph].
- [37] A. M. Sirunyan *et al.* (CMS), *JHEP* **07**, 208 (2021), arXiv:2103.02708 [hep-ex].
- [38] A. M. Coutinho, A. Crivellin, and C. A. Manzari, *Phys. Rev. Lett.* **125**, 071802 (2020), arXiv:1912.08823 [hep-ph].
- [39] A. Crivellin and M. Hoferichter, *Phys. Rev. Lett.* **125**, 111801 (2020), arXiv:2002.07184 [hep-ph].
- [40] V. Cirigliano and I. Rosell, *JHEP* **10**, 005 (2007), arXiv:0707.4464 [hep-ph].
- [41] W. J. Marciano and A. Sirlin, *Phys. Rev. Lett.* **71**, 3629 (1993).
- [42] V. Cirigliano, D. Díaz-Calderón, A. Falkowski, M. González-Alonso, and A. Rodríguez-Sánchez, (2021), arXiv:2112.02087 [hep-ph].
- [43] D. Počanić *et al.* (PiBeta), <http://pibeta.phys.virginia.edu/> (2009).
- [44] E. Frlež *et al.*, *Nucl. Instrum. Meth. A* **526**, 300 (2004), arXiv:hep-ex/0312017.
- [45] D. Počanić *et al.*, *Phys. Rev. Lett.* **93**, 181803 (2004), arXiv:hep-ex/0312030.
- [46] E. Frlež *et al.*, *Phys. Rev. Lett.* **93**, 181804 (2004), arXiv:hep-ex/0312029.
- [47] M. Bychkov *et al.*, *Phys. Rev. Lett.* **103**, 051802 (2009), arXiv:0804.1815 [hep-ex].
- [48] A. Czarnecki, W. J. Marciano, and A. Sirlin, *Phys. Rev. D* **101**, 091301 (2020), arXiv:1911.04685 [hep-ph].
- [49] D. Počanić, E. Frlež, and A. van der Schaaf, *J. Phys. G* **41**, 114002 (2014), arXiv:1407.2865 [hep-ex].
- [50] W. J. Marciano, *Phys. Rev. Lett.* **93**, 231803 (2004), arXiv:hep-ph/0402299.
- [51] J. C. Hardy and I. S. Towner, *Phys. Rev. C* **102**, 045501 (2020).
- [52] R. E. Shrock, *Phys. Lett. B* **96**, 159 (1980).
- [53] R. E. Shrock, *Phys. Rev. D* **24**, 1232 (1981).
- [54] R. Abela, M. Daum, G. H. Eaton, R. Frosch, B. Jost, P. R. Kettle, and E. Steiner, *Phys. Lett. B* **105**, 263 (1981), [Erratum: *Phys. Lett. B* **106**, 513 (1981)].
- [55] R. C. Minehart, K. O. H. Ziock, R. Marshall, W. A. Stephens, M. Daum, B. Jost, and P. R. Kettle, *Phys. Rev. Lett.* **52**, 804 (1984).
- [56] D. A. Bryman, R. Dubois, T. Numao, B. Olaniyi, A. Olin, M. S. Dixit, J. M. Poutissou, and J. A. Macdonald, *Phys. Rev. Lett.* **50**, 1546 (1983).
- [57] G. Azuelos *et al.*, *Phys. Rev. Lett.* **56**, 2241 (1986).
- [58] D. I. Britton *et al.*, *Phys. Rev. Lett.* **68**, 3000 (1992).

- [59] A. Aguilar-Arevalo *et al.* (PIENU), Phys. Rev. D **97**, 072012 (2018), arXiv:1712.03275 [hep-ex].
- [60] A. Aguilar-Arevalo *et al.* (PIENU), Phys. Lett. B **798**, 134980 (2019), arXiv:1904.03269 [hep-ex].
- [61] W. Altmannshofer, S. Gori, and D. J. Robinson, Phys. Rev. D **101**, 075002 (2020), arXiv:1909.00005 [hep-ph].
- [62] J. A. Dror, Phys. Rev. D **101**, 095013 (2020), arXiv:2004.04750 [hep-ph].
- [63] B. Batell, T. Han, D. McKeen, and B. Shams Es Haghi, Phys. Rev. D **97**, 075016 (2018), arXiv:1709.07001 [hep-ph].
- [64] D. Počanić *et al.* (PEN), <http://pen.phys.virginia.edu/> (2006).
- [65] C. J. Glaser *et al.* (PEN), *13th Conference on the Intersections of Particle and Nuclear Physics*, (2018), arXiv:1812.00782 [hep-ex].
- [66] S. Mihara, J. Phys. Conf. Ser. **308**, 012009 (2011).
- [67] T. J. Roberts, K. B. Beard, D. Huang, S. Ahmed, D. M. Kaplan, and L. K. Spentzouris, Conf. Proc. C **0806233**, WEPP120 (2008).
- [68] S. M. Mazza (PIONEER), Instruments **5**, 40 (2021), arXiv:2111.05375 [physics.ins-det].
- [69] G. Pellegrini *et al.*, Nucl. Instrum. Meth. **A765**, 12 (2014).
- [70] M. Tornago *et al.*, Nucl. Instrum. Meth. A **1003**, 165319 (2021), arXiv:2007.09528 [physics.ins-det].
- [71] G. Paternoster, G. Borghi, M. Boscardin, N. Cartiglia, M. Ferrero, F. Ficorella, F. Siviero, A. Gola, and P. Bellutti, IEEE Electron Device Letters **41**, 884 (2020).
- [72] Z. Galloway, C. Gee, S. Mazza, H. Ohldag, R. Rodriguez, H.-W. Sadrozinski, B. Schumm, A. Seiden, W. Wyatt, and Y. Zhao, Nuclear Instruments and Methods in Physics Research Section A: Accelerators, Spectrometers, Detectors and Associated Equipment **923**, 5 (2019).
- [73] M. Andrä *et al.*, Journal of Synchrotron Radiation **26**, 1226 (2019).
- [74] E. Rivera, “Gain suppression mechanism observed in low gain avalanche detectors,” <https://indico.cern.ch/event/983068/contributions/4223231/> (2021).
- [75] “Particulars-tct,” <http://particulars.si/>.
- [76] H. Sadrozinski, <https://indico.cern.ch/event/861104/contributions/4503072/attachments/2306673/3924214/H.Sadrozinski.pdf> (2021).
- [77] E. Olave, F. Fausti, N. Cartiglia, R. Arcidiacono, H.-W. Sadrozinski, and A. Seiden, Nuclear Instruments and Methods in Physics Research Section A: Accelerators, Spectrometers, Detectors and Associated Equipment **985**, 164615 (2021).
- [78] A. M. Baldini *et al.* (MEG), Eur. Phys. J. C **76**, 434 (2016), arXiv:1605.05081 [hep-ex].
- [79] A. M. Baldini *et al.*, Eur. Phys. J. C **78**, 380 (2018).
- [80] R. Onda, “Evaluation of Radiation Damage to VUV-MPPC for MEG II Liquid Xenon Detector,” https://meg.web.psi.ch/docs/talks/JPS/2020s/onda_jps2020s.pdf (2020).
- [81] A. Baldini *et al.*, Nucl. Instrum. Meth. A **545**, 753 (2005), arXiv:physics/0407033.

- [82] R.-Y. Zhu, Proc. SPIE Int. Soc. Opt. Eng. **11838**, 42 (2021).
- [83] N. Atanov *et al.*, Nucl. Instrum. Meth. A **824**, 684 (2016), arXiv:1605.09419 [physics.ins-det].
- [84] R. Mao, L. Zhang, and R.-Y. Zhu, IEEE Trans. Nucl. Sci. **59**, 2224 (2012).
- [85] R. Zou, “The Apollo ATCA design for CMS track finder and pixel readout at the HL-LHC,” indico.cern.ch/event/1019078/contributions/4444387/ (2021).
- [86] “Midas documentation,” www.midas.triumf.ca/MidasWiki/index.php/Midas_documentation (2018).
- [87] “CUDA documentation,” www.developer.nvidia.com/cuda-toolkit (2021).
- [88] “ROOT documentation,” www.root.cern (2021).
- [89] S. Agostinelli *et al.* (GEANT4), Nucl. Instrum. Meth. A **506**, 250 (2003).
- [90] J. Ziegler, J. Biersack, and U. Littmark, *The Stopping and Range of Ions in Solids*, Stopping and ranges of ions of matter (Pergamon, 1985).
- [91] A. A. Aguilar-Arevalo *et al.* (PIENU), Nucl. Instrum. Meth. A **791**, 38 (2015), arXiv:1505.02737 [physics.ins-det].
- [92] G. Bressi *et al.*, Nucl. Phys. B **513**, 555 (1998).
- [93] J. Jaeckel and A. Ringwald, Ann. Rev. Nucl. Part. Sci. **60**, 405 (2010), arXiv:1002.0329 [hep-ph].
- [94] K. S. Jeong, T. H. Jung, and C. S. Shin, Phys. Rev. D **101**, 035009 (2020), arXiv:1811.03294 [hep-ph].
- [95] P. Agrawal and K. Howe, JHEP **12**, 029 (2018), arXiv:1710.04213 [hep-ph].
- [96] D. S. M. Alves and N. Weiner, JHEP **07**, 092 (2018), arXiv:1710.03764 [hep-ph].
- [97] G. B. Gelmini and M. Roncadelli, Phys. Lett. B **99**, 411 (1981).
- [98] Y. Chikashige, R. N. Mohapatra, and R. D. Peccei, Phys. Lett. B **98**, 265 (1981).
- [99] C. S. Aulakh and R. N. Mohapatra, Phys. Lett. B **119**, 136 (1982).
- [100] F. Wilczek, Phys. Rev. Lett. **49**, 1549 (1982).
- [101] A. Aguilar-Arevalo *et al.* (PIENU), Phys. Rev. D **101**, 052014 (2020), arXiv:2002.09170 [hep-ex].
- [102] S. E. Derenzo, Phys. Rev. **181**, 1854 (1969).
- [103] D. A. Bryman and E. T. H. Clifford, Phys. Rev. Lett. **57**, 2787 (1986).
- [104] R. Bilger, K. Foehl, H. Clement, M. Croni, A. Erhardt, R. Meier, J. Patzold, and G. J. Wagner, Phys. Lett. B **446**, 363 (1999), arXiv:hep-ph/9811333.
- [105] R. Bayes *et al.* (TWIST), Phys. Rev. D **91**, 052020 (2015), arXiv:1409.0638 [hep-ex].
- [106] D. Y. Bardin, S. M. Bilenky, and B. Pontecorvo, Phys. Lett. B **32**, 121 (1970).
- [107] T. E. O. Ericson and S. L. Glashow, Phys. Rev. **133**, B130 (1964).
- [108] A. Vanzha, A. Isaev, and L. Lapidus, Sov. J. Nucl. Phys. **12**, 325 (1971), [Yad. Fiz. **12**, 595 (1970)].
- [109] A. Aguilar-Arevalo *et al.* (PIENU), Phys. Rev. D **102**, 012001 (2020), arXiv:2006.00389 [hep-ex].